REPORT SERIES IN GEOPHYSICS
No 81

EFFECTS OF BOREAL FOREST ON MULTI-SCALE OPTICAL REMOTE SENSING OBSERVATIONS FOR SNOW-COVERED LANDSCAPE

Kirsikka Heinilä

Institute for Atmospheric and Earth System Research
Faculty of Science
University of Helsinki
Helsinki, Finland

Academic dissertation in geophysics

To be presented, with the permission of the Faculty of Science of the University of Helsinki, for public discussion in Auditorium 302 of Athena (Siltavuorenpenger 3 A) on 29th of November 2019 at 12 o'clock.

Helsinki 2019

Author's Contact Details

Kirsikka Heinilä
Finnish Environment Institute
Latokartanonkaari 11
00790 Helsinki, Finland
kirsikka.heinila@ymparisto.fi

Supervisors

Professor Matti Leppäranta, Ph. D.
Department of Physics
INAR – Institute for Atmospheric and Earth System Research
University of Helsinki, Finland

Professor Petri Pellikka, Ph.D.
Department of Geosciences and Geography
INAR – Institute for Atmospheric and Earth System Research
University of Helsinki, Finland

Research professor Jouni Pulliainen, Ph.D.
Space and Earth Observation Centre
Finnish Meteorological Institute, Finland

Reviewers

Docent Sirpa Rasmus, Ph.D.
Arctic Centre
University of Lapland, Finland

Docent Stefan Wunderle, Ph.D.
Remote Sensing Group
University of Bern, Switzerland

Custos

Professor Petteri Uotila, Ph. D.
INAR – Institute for Atmospheric and Earth System Research
University of Helsinki, Finland

Opponent

Professor Anne Nolin, Ph. D.
Department of Geography
University of Nevada, Reno

Report Series in Geophysics No 81
ISBN 978-951-51-5624-2 (paperback)
ISSN 0355-8630
Unigrafia, Helsinki 2019

ISBN 978-951-51-5625-9 (pdf)
http://ethesis.helsinki.fi/
Helsingin yliopiston verkkojulkaisut
Helsinki 2019

Cover picture: Boreal forest site in Sodankylä in March 2010.

Abstract

Optical snow monitoring methods have tendency to underestimate snow cover beneath the evergreen forest canopy due to the masking effect of trees. There is need to develop method for providing more reliable snow products and enhance their use e.g. in hydrological and climatological models. The main objective of this thesis is to provide information to improve the accuracy of snow mapping by algorithm development and its regional parameterization. This thesis exploits reflectance data derived from ground-based, mast-borne, airborne and space-borne sensors. Each datatype with different ground resolutions has specific strengths and weaknesses. Together this dataset provides valuable information to advance knowledge of reflectance properties of snow-covered forests and supports the interpretation of satellite-borne reflectance observations. Improvement of satellite-based snow cover mapping is essential because it is the only way to monitor snow cover spatially, temporally and economically effectively.

To obtain information about certain geophysical variable using satellite data, a model for interpreting the satellite signal must be developed. The feasibility of satellite-borne observations in describing geophysical variables depends on the reliability of the model used. Here simple reflectance models based on the zeroth order radiative transfer equation and lineal mixing models are investigated. They are found to reliably describe the observed surface reflectances from snow-covered terrain, both in forests and in open areas. Additionally, to improve methods for seasonal snow cover monitoring in forests, the high spatial resolution observations are required to describe spectral properties and their temporal behaviour of different targets inside the investigated scene. It is also important to combine these target-specific reflectances with the in situ data to describe the characteristics of the target area. In this thesis the datasets complement each other so that while mast-borne data provides information on the temporal behaviour of the scene reflectance of the specific location where measurement conditions are well known, the airborne data provides information during a very short time (~1 hour) on the spatial variation of scene reflectance from the areas where land cover, forest characteristics and snow conditions are well defined. The results demonstrate the notable effect of forest on observed reflectance in both the temporal (changes in illumination geometry) and on

the spatial (changes in forest structure) scale. The presence of tree canopy also weakens the capability of the Normalized Difference Snow Index (NDSI) to detect snow-covered areas. Additionally, the effect of melting snow cover on reflectances and NDSI is significant in all land covers producing high variation inside individual land cover types too.

Keywords: reflectance, scene reflectance, optical, spectra, snow, snow melt, boreal forest, NDSI, multi-scale, canopy cover, land cover, snow mapping, FSC

Preface

This work has been a very interesting journey where it has been possible to combine my geophysical background with my great interest in the environment. I am very grateful of the knowledge I have gained throughout my studies not forgetting field campaigns, which I have had the chance to organize and from what I have enjoyed a lot being an outdoor loving person. Thanks are due to all the people who have been part of this journey. First I want to thank my supervisors Professors Matti Leppäranta from University of Helsinki (UHEL), Petri Pellikka (UHEL) and Jouni Pulliainen from Finnish Meteorological Institute (FMI) who have guided and supported me at every stage of my doctoral studies. Many thanks also to Prof. Petteri Uotila (UHEL) who inherited Matti's position as professor in geophysics. Petteri has given me valuable advice on completing the dissertation.

I am very grateful to Dr. Sari Metsämäki, my unofficial supervisor at the Finnish Environment Institute (SYKE), who has guided me into the secrets of snow cover mapping and given me valuable advice and knowledge during my whole doctoral dissertation. Many thanks to my superiors Sampsa Koponen (SYKE) and Yrjö Sucksdorff (SYKE) who have made it possible for me to carry out this fascinating research and provided a stimulating working environment at SYKE. I also want to express my great gratitude to Prof. Petri Pellikka for giving me the opportunity to be a part of the Airborne Imaging Spectroscopy Application and Research on Earth Sciences (AISARES) graduate school of the University of Helsinki. Additionally, I acknowledge all my co-authors, especially Dr. Miia Salminen (FMI) who has given me golden advice whenever I have needed it, and Dr. Kristin Böttcher (SYKE) for helping me with the field campaigns and especially for the patience to share a room with me. I would like to thank SPECIM (Spectral Imaging Ltd.) and the Väisälä Foundation for supporting this work. I am also very grateful that I have had chance to attend several fascinating field courses and meet many intelligent, lovely people from all over the world. Thanks to exGEO division of SYKE for the amusing and refreshing coffee table discussions and lunch breaks, and also for giving me help and input whenever I needed it. It is always nice to come to work.

I would like to express my sincere thanks to my opponent Prof. Anne Nolin from the University of Nevada (UNR) and to my pre-examiners, Doc. Sirpa Rasmus from the University of Lapland (ULapland) and Doc. Stefan Wunderle from the University of Bern (UniBE), for their time and all comments regarding my dissertation.

I cannot thank my family and friends enough just for being there and being part of my life. My greatest thanks go to Janne and my little sunshines, Vivian and Joel, who make me smile every day and take me totally out of my research bubble. It is so easy to concentrate on the moment with you.

Helsinki, October 2019

Kirsikka Heinilä

Contents

List of appended papers and author´s contribution

This thesis is based on the following five articles, which are referred to in the text by their Roman numerals:

PI. Niemi, K., Metsämäki, S., Pulliainen, J., Suokanerva, H., Böttcher, K., Leppäranta, M., & Pellikka, P. 2012. The behaviour of mast-borne spectra in a snow-covered boreal forest. *Remote Sensing of Environment,* 124, 551-563. doi.org/10.1016/j.rse.2012.06.008

PII. Heinilä, K., Salminen, M., Pulliainen, J., Cohen, J., Metsämäki, S., & Pellikka, P. 2014. The effect of boreal forest canopy to reflectance of snow-covered terrain based on airborne imaging spectrometer observations. *International Journal of Applied Earth Observation and Geoinformation,* 27, 31-41. doi.org/10.1016/j.jag.2013.06.004

PIII. Pulliainen, J., Salminen, M., Heinilä, K., Cohen, J., & Hannula, H.-R. 2014. Semi-empirical modeling of the scene reflectance of snow-covered boreal forest: Validation with airborne spectrometer and LIDAR observations. *Remote Sensing of Environment,* 155, 303-311. doi.org/10.1016/j.rse.2014.09.004

PIV. Heinilä, K., Salminen, M., Metsämäki, S., Pellikka, P., Koponen, S., & Pulliainen, J. 2019. Reflectance variation in boreal landscape during the snow melting period using airborne imaging spectroscopy. *International Journal of Applied Earth Observation and Geoinformation,* 76, 66-76. doi.org/10.1016/j.jag.2018.10.017

PV. Hannula, H.-R., Heinilä, K., Böttcher, K., Mattila, O.-P., Salminen, M., & Pulliainen, J. Laboratory, field, mast-borne and airborne spectral reflectance measurements of boreal landscape during spring. *Earth Syst. Sci. Data Discuss.* doi.org/10.5194/essd-2019-88. In review, 2019.

 Hereafter the publications are referred to by their roman numerals.

This thesis consists of five peer-reviewed papers that are related to the behaviour of optical remote sensing signals observed from a snow-covered boreal forest landscape. In all papers, **PI**–**PIV**, the author acquired, processed and analysed the research data including ground-based, mast-borne and/or airborne spectral datasets. In **PI**, **PII** and **PIV** the author had the main responsibility in all study phases from study planning to the final publication. In these papers the author had the main responsibility to perform the analysis, visualize the results and wrote the papers. In **PV** the author was involved in describing the datasets, doing visualizations and processing the data into publishable form.

List of acronyms and symbols

Acronyms

AISA	Airborne Imaging Spectrometer for Applications
ALS	Airborne Laser Scanning
ASD	Analytical Spectral Devices
BRDF	Bidirectional Reflectance Distribution Function
BRF	Bidirectional Reflectance Factor
CLC2012	Corine Land Cover 2012
ESA	European Space Agency
FMI-ARC	The Arctic Space Centre of the Finnish Meteorological Institute
FOV	Field Of View
FP	Forest parameter
FSC	Fractional Snow Cover
FWHM	Full width at half maximum
GlobSnow	ESA Data User Element (DUE) funded GlobSnow project
GSFC	Goddard Space Flight Center
HDRF	Hemispherical–Directional Reflectance Factor
LiDAR	Light Detection and Ranging
MODIS	Moderate Resolution Imaging Spectroradiometer
NASA	National Aeronautics and Space Administration
NDSI	Normalized Difference Snow Index
NDVI	Normalized Difference Vegetation Index
NIR	Near-infrared
NRT	Near Real Time
SAR	Synthetic Aperture Radar
SCAmod	Snow Covered Area model *i.e.* fractional snow cover retrieval method
SMAC	Simplified method for the atmospheric correction of satellite measurements in the solar spectrum
SWIR	Short-wave infrared
SYKE	Finnish Environment Institute
Terra	NASA's Flagship Earth Observing Satellite
TOA	Top-of-Atmosphere

Symbols

θ_i	Single incidence angle
sd	Snow depth
ϕ	Azimuth angle
R_{obs}	Observed scene reflectance
R_{mod}	Modelled scene reflectance
λ	Wavelength
t	Transmissivity
t^2	The effective, two-way, forest canopy transmissivity
$\rho_{ill.snow}$	Reflectance of directly illuminated snow
$\rho_{shd.snow}$	Reflectance of shadowed snow
ρ_{forest}	Reflectance to describe the canopy reflectance
ρ_{ground}	Snow-free ground reflectance
F_{forest}	Fractional area of tree canopy
$F_{ill.snow}$	Fractional area of directly illuminated snow
FSC	Fractional snow cover
$k_{e,FP}$	Canopy extinction coefficient calculated using forest parameter C, H or V
J	Cost function
i	Sub-index referring to individual observation
r	Correlation coefficient
C	Canopy cover
H	Tree height
V	Product of Canopy cover (C) and Tree height (H)

1. Introduction

1.1 Background and motivation

Over the northern hemisphere extensive areas are covered by seasonal snow cover. The extent of snow fluctuates with the temperature and therefore it is a sensitive climate change indicator. Most of the seasonal snow occurs in the boreal forest region (Figure 1), in which evergreen tree canopy often prevents visibility of the snow layer creating challenges to snow cover mapping by remote sensing instruments (Dietz et al. 2012; Hall and Riggs 2007; Metsämäki et al. 2012). The aim of this thesis is to provide information on the behaviour of reflectance from heterogeneous snow-covered landscape. This information can be directly utilized to improve optical remote sensing methods to provide more reliable information on snow-cover in boreal forests, which also increases the accuracy of the climatological and hydrological models that use these remote sensing retrievals as input.

The significant changes observed in the climate during the past decades have created pressure to increase the effectiveness of environmental monitoring, aiming at better understanding of the processes behind the global warming. Timely detection of changes in the environment – particularly concerning the cryosphere – has a significant role in intervening, resilience and adaptation to undesirable changes in time. Remote sensing is the only effective means to monitor the vast areas on the Earth. However, the economic aspects set limits on the available remote sensing methods. High spatial resolution data is often expensive and covers only small areas at the same time. Thus, high spatial resolution goes often hand in hand with low temporal resolution. Low spatial resolution means that in a heterogeneous landscape one signal is detected from various targets. For environmental monitoring satellite acquisition with short revisiting time is typically exploited: however this provides a pixel size of hundreds of meters or even a few kilometres. When information on a particular target or phenomena is required, a model needs to be developed to interpret the signal.

In optical remote sensing a signal consists of spectral radiances at visible, near-infrared and/or short-wave infrared wavelengths of the electromagnetic spectrum.

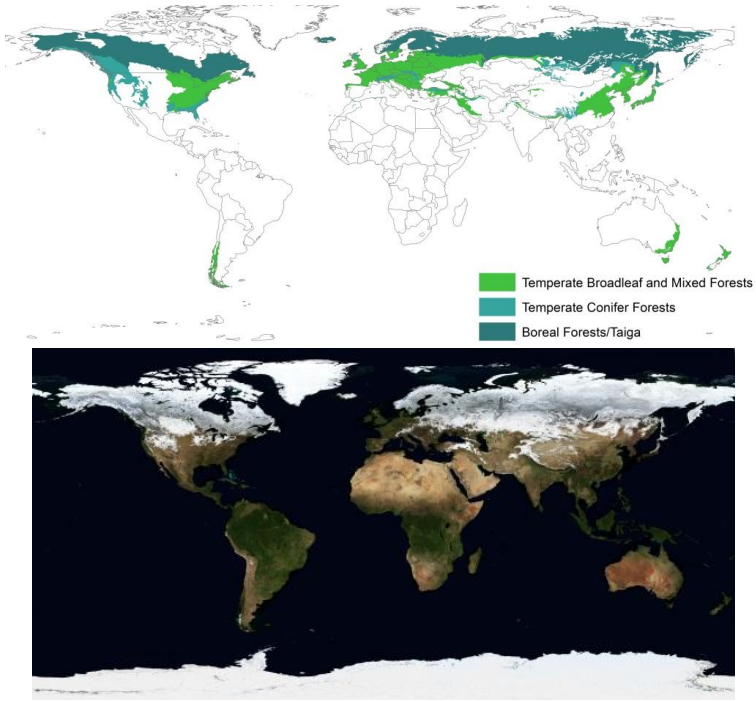

Figure 1. Top: Distribution of boreal, temperate conifer, temperate broadleaf and mixed Forests by The Nature Conservancy (www.maps.tnc.org). Bottom: Snow cover on January 2004 by NASA (www.visibleearth.nasa.gov).

When the electromagnetic radiation interacts with the Earth surface (target), the path of the radiation depends on the target's electromagnetic properties. The most typical measurable optical quantities are reflection, transmission and absorption. The reflected part depends on the directional distribution of incoming radiation, apart from Lambertian surfaces which reflect uniformly in all directions. The directional dependence can be expressed as a bidirectional reflectance distribution function (BRDF). In the field of satellite remote sensing the target surface is often considered to be a Lambertian surface and the reflected part is expressed as bidirectional reflectance factor (BRF) usually referred to as reflectance (Schaepman-Strub et al. 2006). Reflectance, which is the main quantity utilized in this thesis, is the fraction of incident radiation that is reflected by a surface (Figure 2). Mast-borne reflectances measured under full cloud-cover are also utilized, whereby the reflectance can be expressed as Hemispherical–Directional Reflectance Factor (HDRF). Albedo is the measure of surface reflectance to all incoming and outgoing geometries (Figure 2).

The part of the radiation which is not reflected is transmitted or absorbed by the Earth's surface layer. The absorbed energy raises the surface temperature, evaporates water, melts and sublimates snow and ice, and energizes the turbulent heat exchange between the surface and the lowest layer of the atmosphere (Coakley 2003). Albedo has a strong effect on the Earth's energy balance and is a very important parameter in climate models, but cannot be directly measured by satellite sensors (Figure 2).

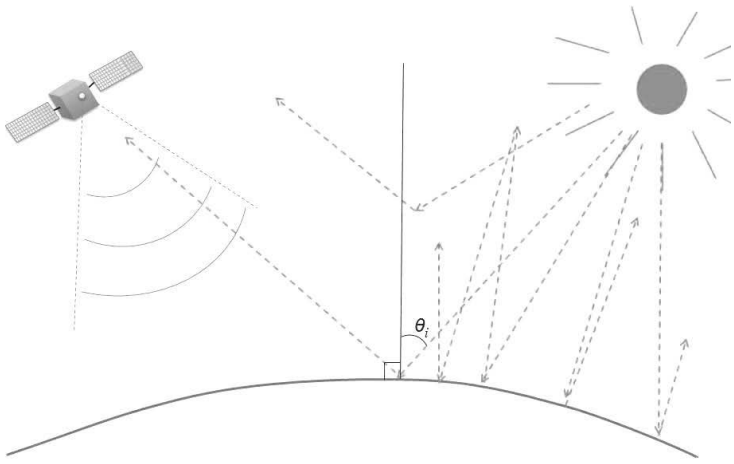

Figure 2. Reflectance is the proportion of incident radiation that is reflected by a surface for a single incidence angle θ_i. Albedo is the directional integration of reflectance over all sun-view geometries and cannot be directly measured by satellite sensors.

Snow cover reflects most of the solar visible radiation and thus it is an important climatological factor. Many previous studies have shown that snow-covered areas decrease especially in the northern hemisphere (e.g. ACIA 2004; AMAP 2011; Chen et al. 2015; Derksen and Brown 2012; Gong et al. 2007; Hori et al. 2017; Jylhä et al. 2004; Malnes et al. 2016; Mellander et al. 2007). Decrease of snow-covered area has a positive feedback on global warming: the increased temperature of the Earth decreases the extent of snow cover which in turn increases the area of snow-free ground where solar energy is absorbed, and thus the land surface that is heated. Snow melting in the north can also cause the melting of permafrost, which stores organic carbon for thousands of years and eventually this carbon is released to the

atmosphere (Turetsky et al. 2019). Seasonal snow cover has also an important role in the hydrological cycle. During the spring melt the large amount of fresh water stored in the snow pack is released causing a high runoff peak. Information on snow cover is important e.g. for agriculture, the hydropower industry and flood prediction. Snow-covered areas in the world are mostly sparsely populated and the amount of available in situ measurements is limited. Thus, hydrological forecasting increasingly combines remote sensing data with hydrological models (Haefner et al. 1997; Solberg and Andersen 1994; Thirel et al. 2013; Winther and Hall 1999).

Unlike most of the other natural targets snow reflects almost all incoming radiation in the visible and near-infrared wavelengths, which is a foundation of several snow remote sensing methods. In open areas like tundra, the determination of snow-covered area is already rather accurate (Hall and Riggs 2007; Metsämäki et al. 2012; Painter et al. 2009; Wang et al. 2017). Though, reflectance data in visible and other optical wavelengths is limited due to cloud cover as well as low light conditions in high latitudes during the polar night. Microwave based methods do not have these limitations, but have their own weaknesses in snow detection. Passive microwave instruments have often coarse resolution (10–20 km) and work suitably only in completely dry snow conditions due to the strong attenuation of microwaves in the wet snow pack (Chang et al. 1990; Kelly et al. 2003; Pulliainen 2006). Active microwave instruments, like SAR, have often fine spatial resolution, but sensors have typically a relatively narrow swath limiting data areal coverage. Active microwave sensors are suitable for wet snow detection, but do not distinguish dry snow from snow-free surfaces and interpretation of SAR data for snow extent mapping in forests is difficult (Nagler et al. 2016; Rondeau-Genesse et al. 2016; Shi et al. 1994). Thus most of the operational snow-mapping methods based on the optical wavelengths.

The semi-empirical reflectance model *SCAmod* exploits optical wavelengths and is utilized in regional and hemispherical scales for mapping sub-pixel fractional snow cover (FSC) (Metsämäki et al. 2005, 2012, 2015). *SCAmod* originates from radiative transfer theory and describes the scene-level reflectance as a mixture of three major reflectance constituents – opaque forest canopy, snow and snow-free ground, which are interconnected through forest canopy transmissivity and snow fraction. However,

in operative use spatially and temporally non-varying constant values for reflectance constituents are typically used i.e. these are not regionally tuned. These constant values are determined from at-ground and space borne spectral measurements (Salminen et al. 2009; Metsämäki et al. 2012). Therefore regardless of canopy transmissivity, information which basically compensates for the effect of forest canopy on the observed reflectances, the FSC retrievals have inaccuracies in regions where these constant values are not representative. Thus, underestimations of FSC may occur, although not as strongly as those produced by many other optical data-based methods in forests where evergreen vegetation decreases the observed reflectance from snow-covered terrain (Coakley 2003; Dietz et al. 2012; Metsämäki et al. 2012; Steele et al. 2017; Turetsky et al. 2019). Underestimation is also a problem in open areas at the end of the melting period when the snow layer is thin and snow-free patches are present (Dietz et al. 2012; Frei et al. 2012; Vikhamar and Solberg 2003; Xin et al. 2012). Additionally, at the end of the melting period the snow layer contains more impurities as a consequence of upper layers melting, which decreases snow reflectance especially in visible wavelengths causing underestimations on modelled FSC (Grenfell et al. 1981; Warren and Wiscombe 1980). Snow grain size is also usually large after melt metamorphosis, increasing forward scattering of snow and decreasing reflectance particularly in the near-infrared region (Dozier et al. 2009; Nolin and Dozier 1993; Painter et al. 1998; Wiscombe and Warren 1980). At the very end of the melting period, satellite observed reflectance can be affected by the reflectance properties of thin melting snow, forest canopy and snow-free patches, resulting in a low observed reflectance and thus differing completely from the spectral behaviour of snow. With respect to the FSC mapping, the usability of satellite data can be improved e.g. by better forward modelling of the behaviour of snow-free ground, the forest canopy and melting snow reflectances. This thesis addresses these problems and provides tools to make snow mapping more accurate also in a heterogeneous snow-covered landscape.

1.2 Objectives

In this thesis, the multisensor data from different ground resolutions are examined in order to improve consideration of forest canopy effects on space-borne remote sensing of snow extent or FSC (Figure 3.). Although the spectral behaviour of snow itself is well known, the combination of spectral properties of snow and forest canopy has been examined less, not to mention the observations combining the spectral properties of snow, forest canopy and snow-free ground. In order to increase the accuracy of FSC retrievals it is crucial to identify the relation of scene-level reflectance to the variation of the natural ground targets' spectral signatures. To define the nature and magnitude of this relation, high resolution measurements in a controlled condition are fundamental. Here the novel and unique experimental hyperspectral datasets are utilized and described in order to depict their significance in the improvement of satellite-borne snow monitoring. The main objectives of the thesis are:

- To examine the effect of snow properties and illumination geometry on scene reflectance through the spring melt by investigating mast-borne spectroradiometer data from a forest site and from forest opening (PI) as well as to analyse the bidirectional reflectance properties of mast-borne observations from a forest site (PI, PII and PIII).
- To examine the effect of forest characteristics on the measured scene reflectance by applying the airborne spectrometer data measured from a rather homogenous dry snow layer and the LiDAR (Light Detection and Ranging) -based canopy characteristics (PII and PIII).
- To examine the effect of snow on canopy on snow-covered terrain reflectance in different types of forests by applying mast-borne and airborne spectral data as well as LiDAR-based canopy characteristics (PI and PII).
- To model the scene reflectance from snow-covered forest using zeroth order radiative transfer approach (PI, and PIII). In PI the combination of linear mixing model and the zeroth-order solution of the radiative transfer equation is employed to model the mast-borne scene reflectance for both mast-borne measurement sites, the forest and the forest opening. In PIII the zeroth order

radiative transfer model is developed and validated to describe snow conditions and simulate the effects of the forest canopy on remote sensing observations using LiDAR based canopy information.

- To investigate the effect of forest canopy and land cover type on spectral properties of snow-covered landscape at the end of the melting period using airborne spectrometer reflectances and LiDAR based canopy coverages and Corine land cover classes (PIV).
- To describe the reflectance datasets observed at multiple scales for boreal landscapes in Finland (PV).

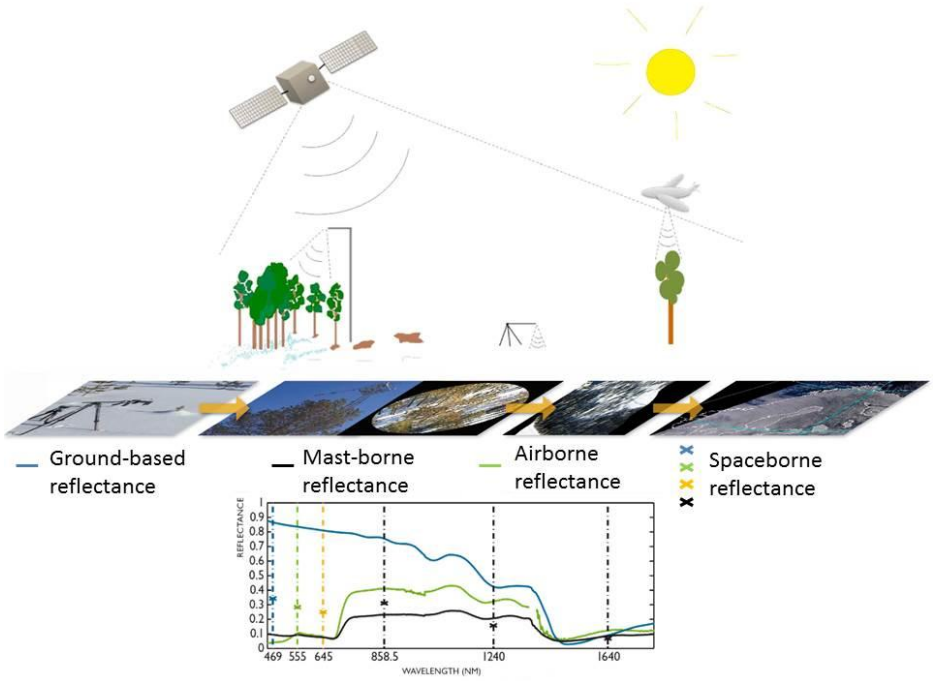

Figure 3. The multisensor reflectance data from different ground resolutions is examined in order to investigate the effect of the tree canopy on remote sensing signals from snow-covered ground. Ground-based reflectance (blue line) represents snow cover, airborne reflectance (green line) of 80cm pixel is measured above the tree crown with under-canopy snow. Mast-borne (black line) and spaceborne (asterisk) reflectances are measured from boreal forest with under-canopy snow.

2. Study area and material

2.1 Study area and measurement campaigns

The measurements were conducted in two study sites in Northern Finland (Figure 4). The first study site is in Sodankylä, at 26.6◦E 67.4◦N, about 100 km north of the Arctic Circle and 180 m above sea level (a.s.l.). The Sodankylä site represents a typical northern boreal landscape with sparse coniferous forest dominating the area, but open wetlands are also present. The second study site is in Saariselkä, 28.2° E 68.3° N, about 200 km north of the Arctic Circle and having the highest point at 718 m a.sl. The timberline in the Saariselkä fell region is at an altitude of 400 m above sea level. The landscape at lower altitudes consists of mires, boreal forests and heaths.

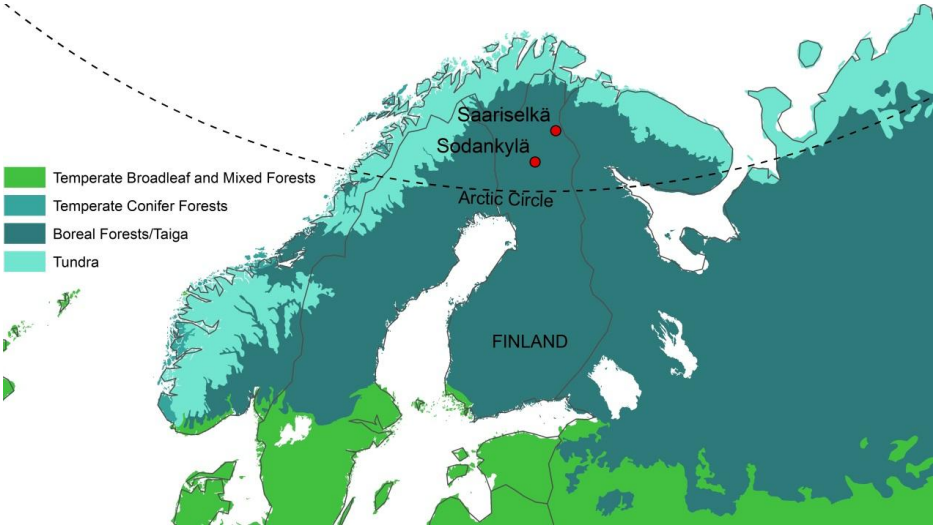

Figure 4. Study sites Sodankylä and Saariselkä in Northern Finland. Distribution of boreal, temperate conifer, temperate broadleaf and mixed forests, and tundra by The Nature Conservancy (www.maps.tnc.org).

The forests in Northern Finland are dominated by Scots pine (*Pinus silvetris*) having a median tree height of 12 m and crown coverage of 30% (Törmä et al. 2011). Typical under-canopy species in Northern Finland are heather (*Calluna vulgaris*), lingonberry (*Vaccinium vitis-idaea*), reindeer lichens (*Cladonia spp.*) and mosses (e.g. *Pleurozium schreberi*). The Sodankylä area has snow cover typically from the

end of October to the middle of May while in the Saariselkä area the snow stays few weeks longer. The solar elevation is low throughout the year having an annual maximum in midsummer (46° in Sodankylä). Because of the polar night, optical satellite images are not usable from November until the middle of February. In Northern Finland, the melting season usually starts at the end of April. Before that the snow layer is rather homogenous (dry and thick snow layer) during the cold and long winter. When thawing starts the melt-freeze metamorphosis causes a distinctive layered structure and ice lenses in the snow pack. The solar elevation and the length of the day increase quickly in late spring inducing a rapid snow melt further accelerated by the increasing absorption of the thin snow and revealing of snow-free ground. The average annual maximum snow water equivalent in Northern Finland is usually 140–200 mm (Kuusisto 1984). The rapid snow melt often causes floods.

The Arctic Space Centre of the Finnish Meteorological Institute (FMI-ARC) is located at the Sodankylä site offering extensive datasets for the research. A unique mast-borne spectroradiometer hosted by FMI-ARC is one important instrument for this thesis. Valuable auxiliary data for the research are air temperature (at 2m), snow surface temperature and snow depth, which are measured next to the mast every minute. In addition, cloud cover is observed every ten minutes in the area. The first airborne remote sensing campaign with AisaDUAL imaging spectrometer was organized in Sodankylä in March 2010 (see PII). At that time the ground was covered by a dry snow layer more than 70 cm thick. This gave an excellent opportunity to investigate the effect of the tree canopy on scene reflectance observed from snow-covered terrain. The airborne measurements were conducted on two days, 18 and 21 March 2010. On both days the measurement time and the snow surface temperatures were about the same, and the sky was cloudless, but on the earlier day the trees were snow-free and the snow on the ground was several days old, while on the later day the trees were partly snow-covered and the snow surface on the ground was fresh snow (Figure 5, Table 1). Another airborne imaging spectrometer campaign was organized in Sodankylä and Saariselkä on 5 May 2011 (see PIV). On that time spring snow melting was already at the very end in Sodankylä (snow depth $sd \leq 30$ cm) and snow-free ground patches were present (Figure 5, Table 1). In Saariselkä, the spring-snow melting was less advanced ($0 < sd$

≤ 60 cm) and snow-free-areas were found only in open areas (canopy cover C < 10%). In Sodankylä, the measurements were made under direct illumination (cloud cover 0/8), while in Saariselkä they were carried out under diffuse illumination (cloud cover 7/8). The results from Saariselkä are discussed in PIV, but are not covered in this summary as the illumination conditions during the measurements in the Saariselkä site deviate from the illumination conditions of optical satellite observations.

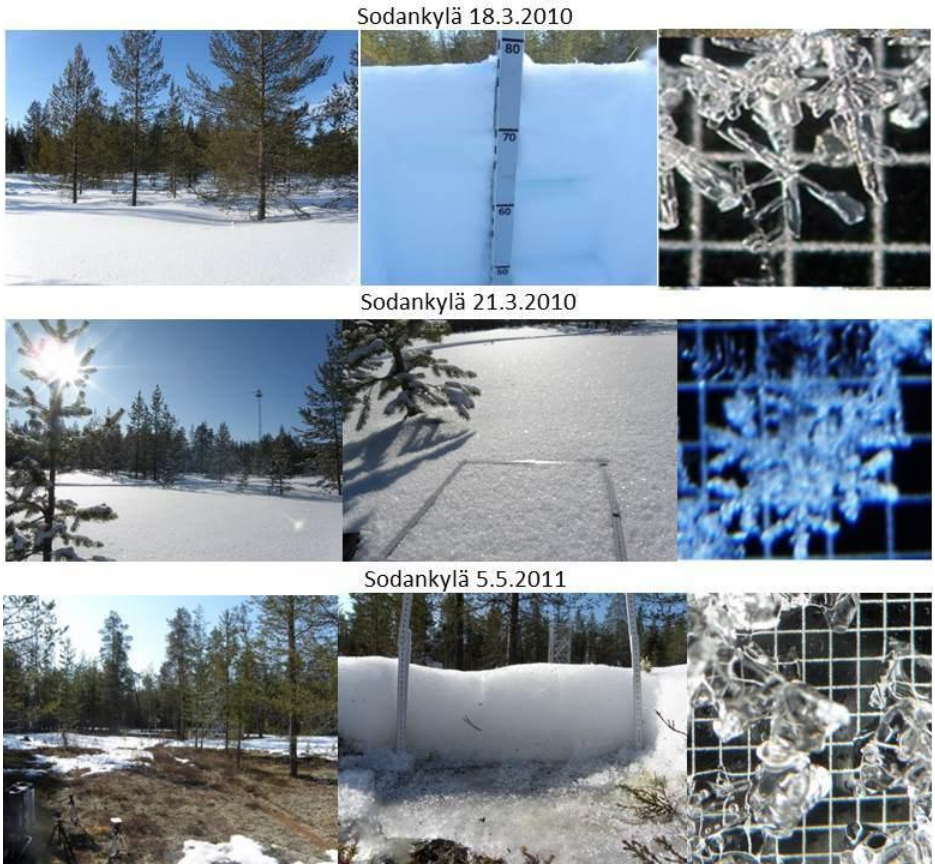

Figure 5. The measurement conditions during the airborne spectrometer flight campaigns in Sodankylä. On 18 March 2010, the canopy was snow-free, snow on the ground (*sd* >70 cm) was dry and the top snow layer was several days old (Top). On 21 March, the canopy was snow-covered, snow on the ground (*sd* >70 cm) was dry and the top snow layer was newly fallen (Middle). On 5 May 2011, the canopy was snow-free, snow on the ground (*sd* < 30 cm) was wet and there were snow-free ground patches (Bottom).

Table 1. The measurement conditions nearby mast-borne spectroradiometer on 18 March 2010, when the canopy was snow-free, on 21 March 2010, when the canopy was snow-covered and on 5 May 2011, when the snow was partly melted.

	18 March 2010 at 10:05 UTC	21 March 2010 at 10:05 UTC	5 May 2011 at 6:45 UTC
Solar azimuth (°)	176	176	122
Solar elevation (°)	22	23	30
Cloud cover (oktas)	0/8	0/8	0/8
Snow depth (cm)	77	83	17
Grain size on top layer (mm)	0.54	0.38	3
Snow-free patches (%)	0	0	60
Snow surface temperature (°C)	-6	-7	0
Air temperature (°C)	-4	-5	7
Snow on canopy	No	Yes	No

2.2 Reflectance data with varying ground resolutions

In this thesis the utilization of multisensor reflectance data from different ground resolution plays a major role. The aerial campaigns provide scene level information on the behaviour of reflectance, which is relevant in parametrization of forward models including canopy and ground components in snow-covered terrain. The spectral information from the ground resolutions between 314 cm^2 to 25 ha gives an opportunity to investigate the effect of single target reflectance characteristics on the scene reflectance from a heterogeneous landscape. This provides tools for the interpretation of reflectance from satellite data, in which spatial resolution is usually hundreds of meters. The spectral datasets and the applications used in the thesis are described in Table 2. This thesis concentrates on the spectral bands and indices which are utilized in widely used snow mapping algorithm SCAmod (Metsämäki et al. 2005, 2012) and in algorithms by NASA's Goddard Space Flight Center (GSFC) (Riggs et al. 2006, 2016). These bands are extracted from the spectra by using the band specific FWHM criterion (Full width at half maximum) corresponding to the spectral channels of the MODIS (Moderate Resolution Imaging Spectroradiometer) instrument on board the Terra satellite. The spectral bands used as well as the band related Normalized Difference Snow Index (NDSI) and Normalized Difference Vegetation Index (NDVI) are presented in Table 3.

Table 2. The utilized datasets and their applications.

Dataset	Original spatial resolution	Regridded spatial resolution	Application
Ground-based spectroradiometer data	341 cm^2	NA	1) Spectral signature of target reflectances in different conditions (PI,PIV,PV) 2) Modelling of scene spectra from forest site and from forest opening (PI)
Mast-borne spectroradiometer data	187 m^2	NA	1) Time series of scene reflectance and indices from forest site and from forest opening (PI) 2) The effect of illumination geometry on scene reflectance from forest site with snow-free and snow-covered canopy (PI, PIII) 3) Performance of NDSI-based snow mapping (PI) 4) Modelling of scene spectra from forest site and from forest opening (PI)
Airborne spectrometer data 80cm	80 × 80 cm^2	NA	1) Behaviour of airborne reflectances or indices in different CLC2012 land cover classes during snow melting (PIV)
Airborne spectrometer data 10m	80 × 80 cm^2	10 × 10 m^2	1) Behaviour of airborne reflectances or indices in different type of forests (PII, PIV) 2) Performance of NDSI-based snow mapping (PII, PIV) 3) Modelling of airborne reflectance as a function of canopy characteristics (PIII)
Satellite data	500 × 500 m^2	NA	1) Performance of NDSI-based snow mapping (PI)

Table 3. Resampled reflectance bands and indices from mast-borne and airborne spectra. The table is adapted from PI ©2012 Elsevier.

MODIS bands	Central wavelength (nm)	Bandwidth (nm)
Band 1	645	620–670
Band 2	858.5	841–875
Band 4	555	545–565
Band 6	1640	1628–1652
MODIS-based indices	Formulation	
NDSI	(Band 4 - Band 6) / (Band 4 + Band 6)	
NDVI	(Band 2 - Band 1) / (Band 2 + Band 1)	

Ground-based data

The ground-based data includes field spectroradiometer measurements, automatic weather station measurements and manual snow pit measurements. The field spectroradiometer measurements are made with a portable Analytical Spectral Devices (ASD) Field Spec Pro JR and the data has been collected since 2006 providing target-specific reflectances for different types of snow and vegetation right after snow melt. Measurements are made in the field in natural conditions. The spectral range of the ASD is 350–2500 nm with 1512 channels. During the measurements the field of view (FOV) was 25°, the mean distance from FOV to the target was 45 cm and the view covered a surface area of 20 cm in diameter. The snow pit measurements were made in each measurement location. Additionally, digital photographs of the surface snow sample, cloudiness, and landscape were taken. Details of the measurement set-up are described in Salminen et al. (2009).

Ground-based reflectances give valuable information on the spectral properties of the one specific target, which is not possible to retrieve with instruments with spatial resolution of tens or hundreds of meters. Prevailing measurement conditions, e.g. snow properties and illumination, are easy to define accurately which makes the data valuable. Having an idea of spectral behaviour of singular targets aids in interpreting the reflectance observed by satellite. In this thesis the fore optic of spectroradiometer was set to observe at nadir direction to reduce the effect of illumination geometry.

This is not always the orientation of satellite instruments which measure the target with a varying viewing angle. Snow and vegetation are anisotropic surfaces and thus are sensitive to illumination geometry. Snow is typically an anisotropic forward scattering surface type and vegetation is backward scattering.

Mast-borne data

The spectroradiometer, similar to the portable instrument utilized for ground-based reflectance measurements, monitors a pine forest and forest opening with cast shadows from pine trees from a 30 meter high mast (Figure 6). Differing from ground-based measurements the instrument was set to look 11° off the nadir, the FOV was the same 25°, while the view covered an area of 187 m^2. The details of the utilized measurements are presented in PI and measurement setup in Sukuvaara et al. (2007). Mast-borne data includes average reflectance spectra from both measurement sites, forest and forest opening, as well as simultaneously acquired digital images, which allows the determination of e.g. the amount of shadows and snow-free patches (Figure 6). The ground layer is characterized by various lichen and moss species on mineral soil.

The mast-borne reflectances, measured above the tree canopy, give a rare opportunity to investigate the behaviour of scene reflectance of a specific forest area from mid-winter to spring. For example, even with high resolution satellite data, the footprint of the instrument varies making it impossible to get time series from exactly the same geographical land surface. In the site observed by the mast-borne spectroradiometer, the tree canopy structure is assumed to be constant throughout the year. Therefore, both in the forest and in the forest opening, snow properties and illumination geometry are the main variables during full snow coverage. This dataset provides useful information for determining the temporal variation of scene reflectance in snow-covered forested terrain. In direct illumination conditions, it is difficult to define which of the changes in observed reflectance are caused by the variations in illumination geometry and which are caused by the variations in snow properties. In addition, the amount of shadows has a considerable effect on the observed scene reflectance. During one single day, when the temperature is below zero degrees Celsius, the snow layer could be assumed to stay rather homogenous.

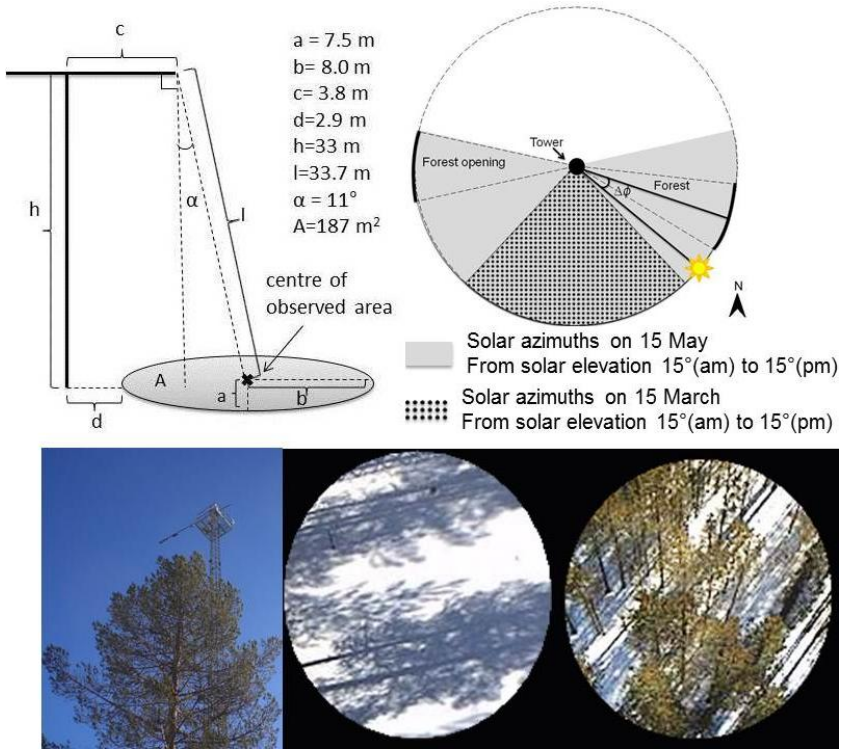

Figure 6. Top left: Spectroradiometer is installed on the top of 30-metre high mast and observes an area of 187°. Top right: Field of view of the forest area and the forest opening as well as solar azimuths between solar elevation 15° (am) and 15° (pm). $\Delta\phi$ defines the azimuth angle difference between the instrument look angle and the sun. Bottom: Spectroradiometer provides average reflectance spectra from the forest area and forest opening as well as simultaneously acquired digital images. This figure is adapted and modified from PI ©2012 Elsevier.

This hypothesis was applied in PI and PII, where the effect of solar elevation, solar azimuth and amount of shadows are investigated during one day. Snow reflects more in the forward direction (e.g. Painter and Dozier 2004; Peltoniemi et al. 2005a) while vegetation has more backscattering behaviour (e.g. Eklundh et al. 2007; Pellikka et al. 2000; Peltoniemi et al. 2005b; Walter-Shea et al. 1997). This makes the modelling of scene reflectance of snow-covered forested terrain difficult with varying illumination and imaging geometries. This is a highly valuable dataset to increase knowledge of the spectral characteristics of scene reflectance where the signal consists of information on objects whose BRDF differ considerably from each

another. However, the data covers only a specific forest site with a sensor zenith angle of 11° and cannot be generalized to be accurate in all kind of boreal forests and with different sensor zenith angles. The measurements during diffuse illumination, i.e. full cloud cover, can be assumed to be only negligibly affected by the changes in illumination conditions and allowed to investigate the effect of snow characteristics on scene spectra. This data aids understanding of the impact of snow properties on scene spectra, also in the area where about half of the area is covered by the tree canopy. Additionally it provides tools to specify the effect of snow properties on scene reflectance observed during direct solar illumination. Though, the effect is not the same when the incident solar radiation comes from single incidence angle compared to hemispherical illumination. The effect of the solar incidence angle is discussed in Nolin and Dozier (1993), where method based on hyperspectral data to estimate snow grain size had a higher accuracy for solar incidence angles between 0° and 30°.

Airborne data

The airborne spectral measurements were made with the AisaDUAL Airborne Imaging Spectrometer for Applications (AISA) from a helicopter in 2010 and from an airplane in 2011. The instrument was set to look at nadir having a FOV of 17°. As both campaigns were done at an altitude of 800 meters (Figure 7), the spatial resolution is 80 cm and swath 240 meters. The spectral range of AisaDUAL is 400 – 2500 nm with 359 channels. The datasets from 2010 and 2011 are described in more detailed in PII and PIV, respectively. The measurement conditions during the campaigns are described in section 2.1.

LiDAR data (Light Detection and Ranging) was acquired by the National Land Survey of Finland. The LiDAR data were utilized to define three height and canopy cover (C) in grid cells of 10 m by 10 m (Cohen et al. 2015). The synergistic utilization of high spatial resolution data of both the LiDAR -based forest characteristics and the airborne reflectances acquired under dry thick snow cover conditions offers a unique possibility to investigate the effect of canopy characteristics on reflectance of snow-covered terrain (Figure 8). This data provides information on the spatial variation of scene reflectance in snow-covered forested

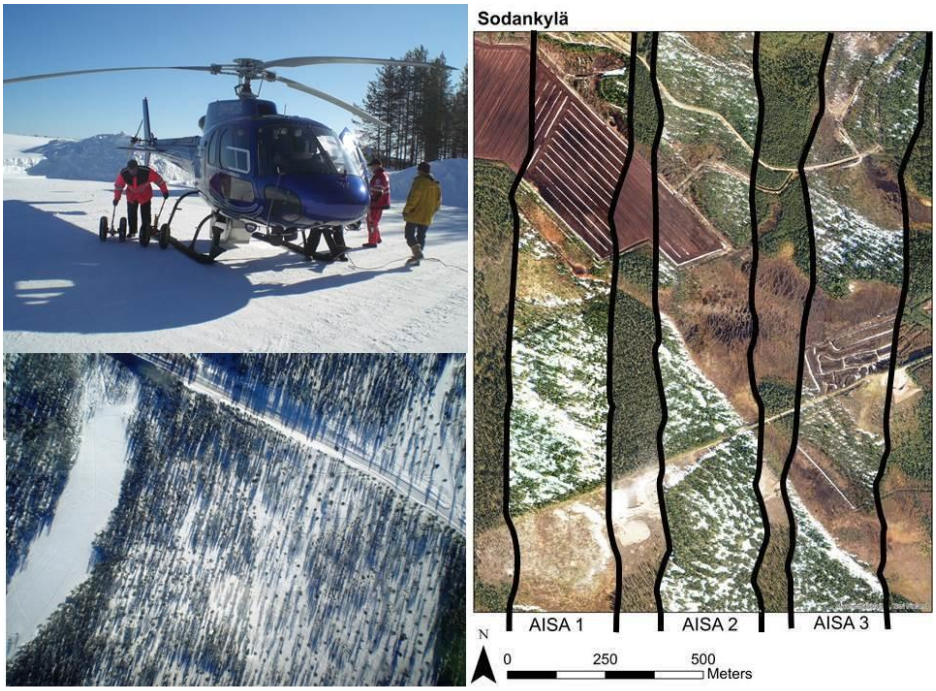

Figure 7. Top left: The hyperspectral remote sensing data acquisition was made from a helicopter in 2010. Bottom left: Snow-covered landscape on 21 March 2010. Right: RGB true colour images of sections of three AISA flight lines on 5 May 2011. Background image is an orthophoto by the National Land Survey of Finland from summer time conditions (This figure is adapted from PIV, ©2019 Elsevier).

terrain and offers valuable information on model development concerning the complex canopy-ground component. Additionally, the airborne data from 2010 enables the effects of snow on the forest canopy on scene reflectance in different types of forests to be investigated, since on the first measurement day the forest canopy was snow-free and on the second measurement day it was snow-covered. A divergent factor was the different optical snow grain size: on 18 March the snow was several days old while on 21 March snow was fresh (see Figure 5). The illumination conditions on these two days are rather similar due to similar flight routes and the same acquisition time (Table 4). The high resolution AISA data from 5 May 2011 offered a valuable opportunity to investigate the effect of a heterogeneous melting snow layer on scene reflectance in different kinds of landscapes. The data were combined with the LiDAR-based canopy cover (C) data and Corine land cover

classification (CLC2012). In Finland CLC2012 data is produced with a ground resolution of 20 by 20 metres (Härmä et al. 2015; Törmä et al. 2011). The most common CLC12 land cover classes at the study sites were utilized to investigate the effect of landscape on reflectances and indices. The detailed information on snow properties, such as snow depth, would have been valuable to assess the effect of snow characteristics on scene reflectance, but was considered too labour-intensive. However, several snow pit measurements were made in the measurement area to obtain an overview of the snow characteristics. The airborne data with high spatial resolution (80 cm) from the end of the snow melting is utilized to investigate the spatial variation of reflectance between snow-covered or snow-free ground areas. However, the snow-free patches surrounding the tree trunks on otherwise snow-covered terrain were hard to capture from the aerial data. On 5 May 2011, the sun elevation was higher than in March 2010 and varied more during the data acquisition. The variation was not considered significant as it was at a maximum of 4.2°. The FOV of AISA observations was 17° meaning that the imaging angles limits to near-nadir angles (0°–8.5° off nadir). The angle between flight direction and sun azimuth may cause variation to the observed reflectances due to both backscattering and forward scattering geometries (Table 4).

Table 4. Solar position and flight direction during the Sodankylä data acquisition on 18 March 2010, on 21 March 2010 and on 5 May 2011; cloud free conditions. BW refers to the case where solar radiation comes backward and FW when it comes forward relative to the flight direction.

Date	Time (UTC)	Sun Elevation (°)	Sun Azimuth ϕ (°)	Flight direction α (°)	$\phi - \alpha$ (°)
2010/3/18	11:00	21.5	190	0 (south to north)	190 (BW)
2010/3/18	11:42	20.3	102	45	157 (FW)
2010/3/18	10:51	21.7	187	100	87 (FW)
2010/3/18	12:05	19.7	206	320	–114 (FW)
2010/3/21	10:45	21.4	203	0	203 (BW)
2010/3/21	10:51	22.8	187	45	142 (FW)
2010/3/21	10:12	23.0	178	100	78 (FW)
2010/3/21	11:16	22.3	195	320	–125 (FW)
2011/5/5	6:13	26.5	113	0	113 (FW)
2011/5/5	6:19	27.0	114	0	114 (FW)
2011/5/5	6:30	28.0	117	0	117 (FW)
2011/5/5	6:02	25.5	110	20	90 (FW)
2011/5/5	6:50	29.6	122	20	102 (FW)
2011/5/5	6:35	28.4	118	45	73 (FW)

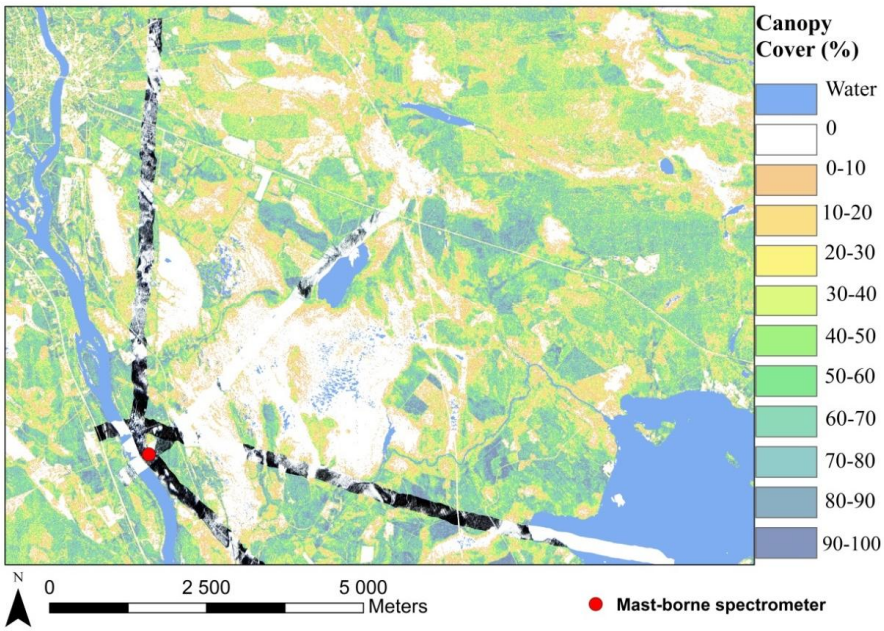

Figure 8. AISA flight lines on 18 March 2010. Similar flight lines were acquired on 21 March 2010 and on 5 May 2011. On the background is the forest canopy cover map derived from the LiDAR data. This figure is adapted from PII, ©2014 Elsevier.

Satellite -borne data

The satellite reflectances are only utilized to demonstrate the capability of NDSI to detect snow-covered areas in forest, since the main objective is to investigate the reflectance properties of snow-covered forests with high resolution data. The 500 meter resolution MODIS image acquired on 28 March 2003 was used, since ground observations on snow depth and coverage as well as Snow Water Equivalent -map (ESA DUE GlobSnow SWE data record, www.globsnow.info) indicated that the terrain was snow-covered on that day. The sub-scene of the MODIS image used presents dense forest along the Finnish-Russian border, visible also in the 30 meter resolution Landsat/ETM+ image acquired on 15 March 2003 (186/017). The purpose of this comparison was to demonstrate the method performance without going into detailed investigations. Thus these results cannot be generalized or used for other illumination conditions (Cao and Liu 2006; Gutman 1991).

3. Analysis and results

3.1 Effect of boreal forest on scene-level reflectance of snow-covered surface

The modelling approach follows the *SCAmod* reflectance model employed in hemispherical snow mapping of fractional snow-covered area at the Finnish Environment Institute (SYKE) (Metsämäki et al. 2005, 2012). The fundamental idea of the approach is to retrieve the signal from the ground beneath the canopy layer by eliminating the influence of tree canopy on the observed signal. In *SCAmod* the observed scene reflectance R_{obs} is described as a function of reflectances of directly illuminated snow $\rho_{ill.snow,}$ snow-free ground ρ_{ground} and opaque tree canopy ρ_{forest} at a certain wavelength λ. The effective two-way canopy transmissivity t^2 is utilized to describe the forest canopy effect on the observed reflectance as a partially transparent layer. The model describes the satellite observed reflectance as follows:

$$R_{\lambda,obs}(FSC) = \left(1 - t_\lambda^2\right)\rho_{\lambda,forest} + t_\lambda^2\left[FSC\ \rho_{\lambda,ill.snow} + (1 - FSC)\ \rho_{\lambda,ground}\right] \quad (1)$$

During full snow cover (FSC=1) Eq. 1 enables the calculation of pixel transmissivity as it forms to

$$R_{\lambda,obs} = \left(1 - t_\lambda^2\right)\rho_{\lambda,forest} + t_\lambda^2\ \rho_{\lambda,ill.snow} \quad (2)$$

MODIS Band 4 (555 nm) reflectance data is most commonly utilized as an input in operational production, but the method is applicable for different sensors and spectral bands. Compared to many other techniques, where forest canopy is defined as an opaque layer, *SCAmod* detects snow more accurately in forested regions, but tends to underestimate snow cover in forests (Metsämäki et al. 2012; Salminen et al. 2018). In PI, this problem is approached by refining the model to describe mast-borne spectra in forest and forest opening for wavelengths 350–1800 nm in fully snow-covered conditions. In addition to $\rho_{ill.snow}$ and ρ_{forest}, the reflectance of shadowed snow $\rho_{shd.snow}$ is applied in the model. The areal proportion of directly illuminated snow $F_{ill.snow}$ is determined from high-resolution digital images for each measurement separately (Figure 9). The dataset consists of 75 measurements from the forest site and 26 measurements from the forest opening measured during fully

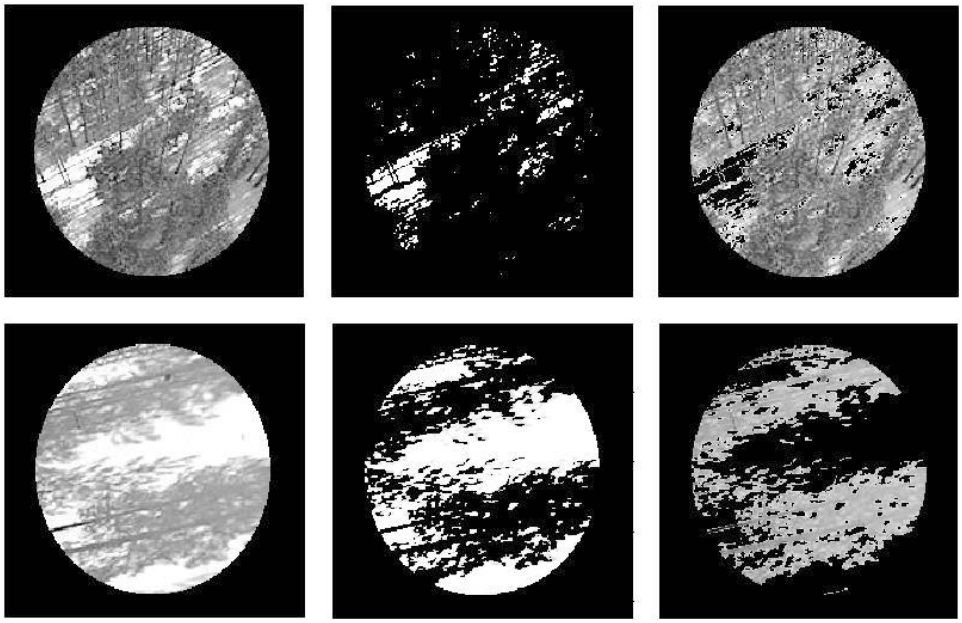

Figure 9. Determination of the directly illuminated area from the digital image. The upper images represents the forest site and the lower ones the forest opening with tree-cast shadows. Left: The blue band image from the observed areas. Middle: Pixels classified as directly illuminated snow. Right: The remaining pixels including (trees/shadows). This figure is adapted from PI, ©2012 Elsevier.

snow-covered ground with a snow depth of more than 40 cm and cloud-free conditions. The model used for the forest site is:

$$R_{\lambda,mod} = F_{ill.snow}\rho_{\lambda,ill.snow} + (1 - F_{ill.snow})[t_\lambda \rho_{\lambda,shd.snow} + \left(1 - t_\lambda^2\right)\rho_{\lambda,forest}] \quad (3)$$

and for the forest opening

$$R_{\lambda,mod} = F_{ill.snow}\rho_{\lambda,ill.snow} + (1 - F_{ill.snow})\rho_{\lambda,shd.snow} \quad (4)$$

The last term of Eq. 3 $\left(1 - t_\lambda^2\right)\rho_{\lambda,forest}$ results from the zeroth-order solution of the radiative transfer equation (Metsämäki 2013). In P1, the reflectance of an opaque forest canopy ρ_{forest} is estimated from the reflectance measurements of pine branches in laboratory conditions (see details of laboratory measurements in PV). $\rho_{ill.snow}$ and $\rho_{shd.snow}$ are determined for both, dry (snow surface temperature T <0°C) and wet (T ≥0°C) snow, due to their different spectral behaviour (Dozier et al. 2009; Rasmus

2005; Salminen et al. 2009; Warren 1982), as well as their weighted mean (see PI). When modelling the mast-borne spectra the forest transmissivity is *a priori* unknown in Eq. 3, enabling the determination of constant values for transmissivity by fitting the model (3) into the mast-borne reflectance spectra. The constant values for transmissivity are estimated for three wavelength intervals 350–699 nm, 700–1349 nm, 1350–1800 nm by minimizing the root mean square error between the modelled and observed scene reflectance measurements. The justification for the utilization of different constant values for these intervals was based on the literature where plant tissue transmittance was indicated to diverge in different wavelength regions (e.g. Knipling 1970; Mesarch et al. 1999; Woolley 1971; Zarco-Tejada et al. 2004). For comparison, the linear mixing model is tested for the forest site as following

$$R_{\lambda,mod} = F_{ill.snow}\rho_{\lambda,ill.snow} + \left(1 - F_{ill.snow} - F_{forest}\right)\rho_{\lambda,shd.snow} + F_{forest}\rho_{\lambda,forest} \qquad (5)$$

Where F_{forest} is the areal proportion of forest canopy to the entire scene area. Results in PI from the forest site shows that the modelling approach combining zeroth order radiative transfer equation and linear mixing model (Eq. 3) describes the light propagation and reflection effects of tree canopy better than the linear mixing model (Eq. 5) (Figure 10). In the forest opening, where only the linear mixing model is utilized, the model predicts higher reflectances in the visible wavelengths and lower reflectances in near-infrared (NIR) wavelengths. This demonstrates the effect of forest transmission on the observed reflectance in open areas too if tree shadows are present.

PI provided valuable information of the effects of forest canopy on scene reflectance, particularly on tree-cast shadows. Unfortunately the shadowed area cannot be defined without very high resolution images, which hampers the investigations of satellite images. In PII, the relation of scene reflectance and canopy cover using high resolution data for both datasets is investigated, because the amount of shadows is related to canopy cover. The airborne measurements with a rather homogenous snow layer (mid-winter in Lapland, several minus degrees and over 70 cm thick snow layer) and cloud-free sky provided suitable conditions for the investigation. The parameters utilized to describe forest characteristics are canopy cover (C), tree height (H) and the product of them, V = C × H, which is related to the forest volume

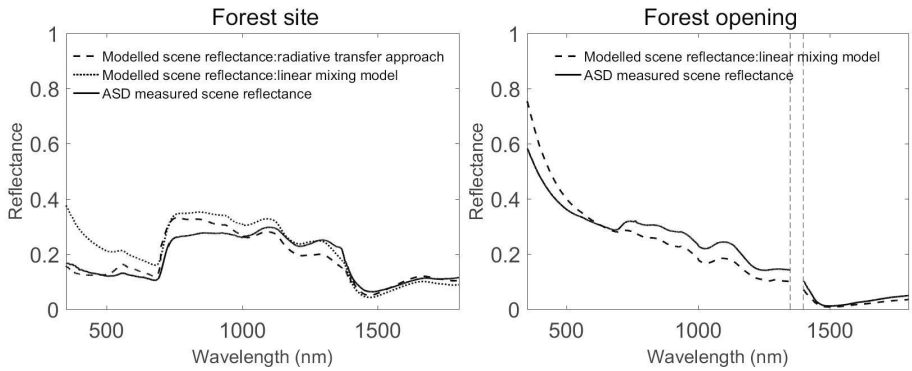

Figure 10. Observed and modelled average mast-borne spectra at full snow cover conditions (*sd* > 40 cm) and with direct illumination. The forest site features 75 observations (Eq. 3 and Eq. 5) and the forest opening partially shadowed by trees features 26 observations (Eq. 4). These figures are adapted and modified from PI, ©2012 Elsevier.

(m^3/ha) and the forest biomass, see PII. The results in PII indicate the strong effect of C and V on the observed reflectance. In dense forests (C of 75–100%), in which the area of directly illuminated snow can be assumed to be close to zero (sun elevation angle was 22°), the reflectance is similar regardless of C (Figure 11). The exponential correlation between reflectance and C or V is notable especially in the case of the green band (555 nm). These results point out the importance of the utilization of a radiative transfer model to describe the behaviour of reflectance in forest with under-canopy snow. Since models which are utilized in near real-time (NRT) monitoring of extensive areas cannot be very complex, the results of PII encourage us to apply a simple radiative transfer approach to describe the scene reflectance at 555 nm as a function of Forest Parameter (FP) C, H and V. In PIII, the semi-empirical reflectance model (Eq. 2) is derived from zeroth order radiative transfer equation so that

$$t_\lambda^2 = \exp(-2\kappa_{e,C} g'(\theta_i) FP) \tag{6}$$

and

$$R_{\lambda,obs} = \left(1 - exp\left(-2\kappa_{e,C} g'(\theta_i) C\right)\right)\rho_{forest} + exp\left(-2\kappa_{e,C} g'(\theta_i) C\right)\rho_{ill.snow} \tag{7}$$

Where $\kappa_{e,FP}$ is the canopy extinction coefficient and θ_i is the angle of incident radiation. The Eq. (7) is utilized in PIII to approximate $\kappa_{e,FP}$, $\rho_{ill.snow}$ and ρ_{forest} by fitting the model into the same airborne observations as utilized in PII by applying a numerical inversion method. The assumption is that these three parameters can be approximated by their mean effective values over the image scene. The model is fitted to airborne observations by using the least squares method minimizing the following cost function *J* with respect to $\kappa_{e,FP}$, $\rho_{ill.snow}$ and ρ_{forest}:

$$J(\kappa_{e,FP}, \rho_{forest}, \rho_{ill.snow}) = \sum_{i=1}^{N} \left(R_{mod,i}(\kappa_{e,FP}, \rho_{forest}, \rho_{ill.snow}, C_i) - R_{obs,i} \right)^2 \quad (8)$$

where sub-index *i* refers to an individual observation case. Additionally, the effect of spatial scale on the results is investigated by estimating the same parameters for airborne imaging spectrometer data with 10 m spatial resolution and for data which is resampled with a two-dimensional box convolution function (10 ×10 window) to a resolution of 100 m (Figure 12). The results in PIII indicated the slight effect of spatial resolution on the modelled parameters. However, the radiative transfer model according to (Eq. 7) describes the behaviour of reflectance in snow-covered landscape well, suggesting the validity of the modelling approach to describe the influence of forests when using instruments with varying spatial resolution (Figure 12). In PIII, it is also confirmed that the radiative transfer approach has a higher validity to describe the scene reflectance than the following linear mixing model.

$$R_{mod} = C\rho_{forest} + (1 - C)\rho_{ill.snow} \quad (9)$$

The correlation coefficient r^2 between the observed and modelled reflectance using the radiative transfer approach (Eq. 7) is as high as 0.91 for all data points processed to 100 m spatial resolution, whereas for the linear mixing model (Eq. 9) r^2 is 0.87. These results indicate that the radiative transfer method (Eq. 7) estimates the attenuation of electromagnetic radiation caused by forest canopy with a good accuracy and is thus suitable to describe snow conditions in forests. Though, in PIV the airborne reflectances measured over thin melting snow layer are investigated and it was found that the relation between C and visible reflectance (555 nm and 648 nm) is not clearly exponential when the snow layer is thin and partially transparent (Figure 11). This is caused by the high internal variation of reflectances especially within canopy cover of less than 50%.

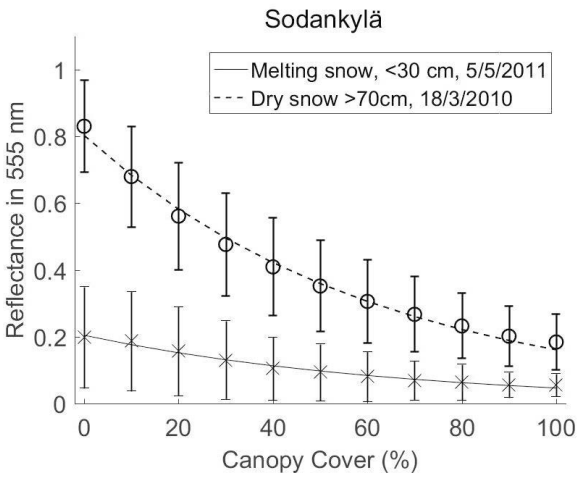

Figure 11. The mean green band reflectance and standard deviation in the case of thin and thick snow pack with respect to canopy cover (%) measured in Sodankylä under direct illumination. During the flights on 18 March 2010 the solar elevation θ was 22–23°C and on 5 May 2011 θ was 26–30°C. This figure is adapted from PIV, ©2019 Elsevier.

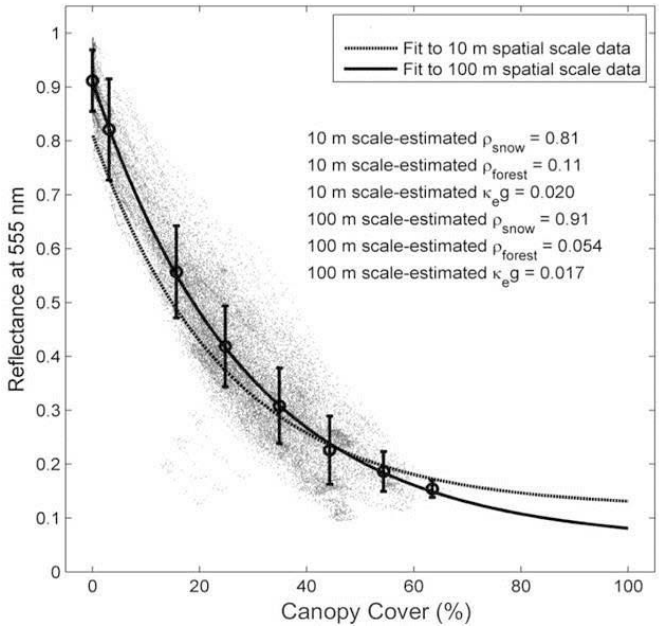

Figure 12. Modelled (Eq. 7) airborne reflectances as a function of canopy cover for data averaged to a spatial resolution of 100 m at the green band (555 nm) during full snow cover conditions (*sd* > 40 cm) and at direct illumination. Individual data points are depicted by grey dots, whereas the error bars show the standard deviations from class stratified mean values. For comparison the model fitting at a scale of 10 m is also shown (dotted curve). The case *C*=0% is excluded from the fitting procedure (Eq. 8).This figure is adapted from PIII, ©2014 Elsevier.

3.2 Capability of NDSI-based techniques to detect snow in boreal forest

NDSI is widely utilized in snow mapping (Coakley 2003; Frei et al. 2012; Hall and Riggs 2007; Hendriks and Pellikka 2004; Niittynen et al. 2018; Panday et al. 2014; Salomonson and Appel 2006; Steele et al. 2017; Turetsky et al. 2019). The operational snow mapping at SYKE also utilizes NDSI as supplementary information to *SCAmod* to identify snow-free areas; this ensures that the increasing green reflectance of the appearing green vegetation is not falsely interpreted as snow by the model. The criterion is the following: if NDSI < −0.1, FSC is set to zero, otherwise FSC is modelled with *SCAmod* (Metsämäki et al. 2012). In PI, the mast-borne spectroradiometer data are exploited in the investigation of the behaviour of NDSI during the spring in two areas: forest and forest opening. The dataset allows investigation of the reflectances measured under cloud-free conditions and under full cloud cover, and thus to discriminate between the effects caused by the variation in illumination conditions and variations in the actual snow characteristics. The results indicate a clear difference between the behaviour of NDSI in the forest compared to the forest opening (Figure 13). In the forest opening the NDSI is similar in both illumination conditions, direct (i.e. clear sky) and diffuse (i.e. full cloud cover), while in the forest the NDSI difference is notable. This indicates that the NDSI is neither sensitive to the variation in illumination conditions nor to the amount of shadows in fully snow-covered areas, but in forests the variation in illumination causes high variation in NDSI. The mast-borne data allowed investigation of this phenomenon with a stable viewing geometry, canopy presence and snow conditions during one single day (18 March 2010) when the main varying variable was the illumination geometry (17°< solar elevation <22°). The dataset gives clear results of the high variability of NDSI (-0.1–0.1) according to the illumination geometry when both snow and forest canopy are present and stable. In PII, the effect of forest characteristics on the variation of NDSI was investigated. The airborne measurements were done at nadir within one hour under clear sky and a fairly homogenous dry snow layer. The results in PII show that the relation between NDSI and C or V is linear. In addition, the results indicate that the NDSI varies significantly (relative variation > 100%) in dense forests, but very little in open areas (Figure 14). According to the time series analysis (Figure 13) the main factor

affecting the NDSI in the forest opening before snow-free patches appear, is the snow optical grain size. There is a slight increasing trend in NDSI time series during the spring when grain size increases during the melting process. However, the most notable effect of snow grain size on NDSI is noted on the days of new snow, when NDSI decreases noticeably in the forest opening. This is due to the small optical grain size of new snow (e.g. Marshall and Oglesby 1994), which increases reflectance more in the infrared region than in the visible region (Dozier et al. 2009; Negi et al. 2010; Nolin and Dozier 2000; Painter et al. 1998; Warren 1982). However, the impact of grain size on NDSI is negligible compared to the effects caused by forest canopy. This is also seen in time series on 21 March 2010 when the new snow layer also covers the tree canopy increasing the NDSI notably on that specific day.

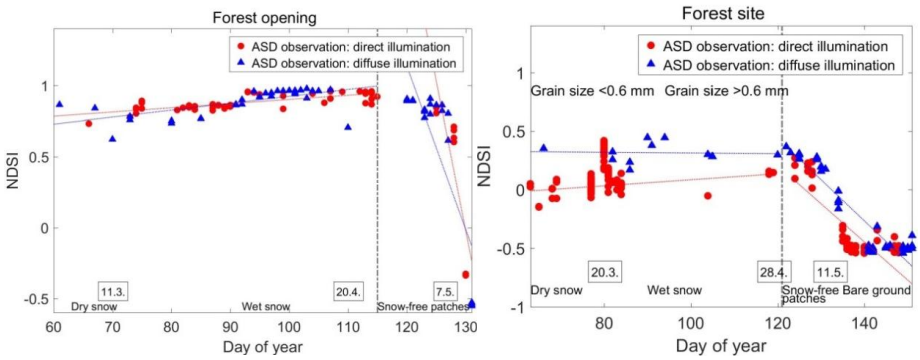

Figure 13. NDSI time series as measured by the mast-borne spectroradiometer under direct or diffuse solar illumination from the forest site. The boxes represent the snowfall dates and vertical dashed line the date when snow-free patches started to appear. Left: The forest site from 4 March to 31 May 2010. Right: The forest opening from 2 March to 11 May 2011. These figures are adapted from PI, ©2012 Elsevier.

Both the mast-borne and the airborne datasets also provide some negative NDSI values in forests, even with snow layer of over 70 cm on the ground. In the recent NASA's MODIS Collection 6, the threshold for NDSI is set to 0.1 in order to classify pixel as snow-covered pixel in NDSI_snow_Cover product (Riggs et al. 2016). A detected pixel with an NDSI between 0 and 0.1 is reversed to a 'not snow' result and bit 2 of the NDSI_Snow_Cover_Algorithm_Flags_QA is set to enable the

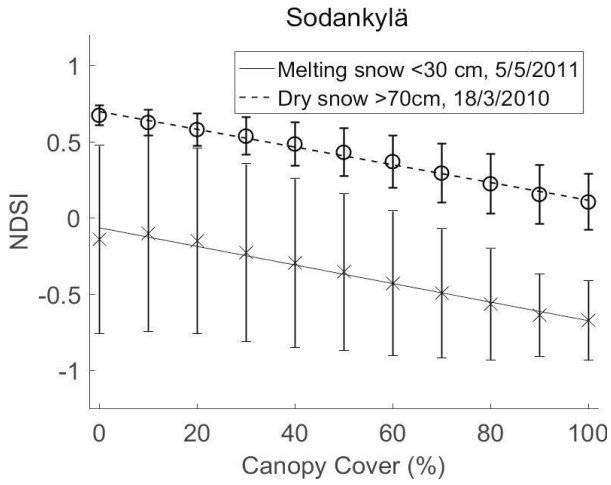

Figure 14. Mean and standard deviation of NDSI with respect to canopy cover (%) measured in Sodankylä under direct illumination and with thin melting (solid line) and dry thick (dashed line) snow pack on the ground. This figure is adapted from PII, ©2014 Elsevier.

user to generate a locally-tuned algorithm (Riggs et al. 2016). In previous Collection 5 (Riggs et al. 2006) the threshold for NDSI is set to between 0.1 and 0.4 in order to classify pixel as a snow-covered pixel depending on the value of NDVI, but this is found to be too low a threshold to capture snow in forests e.g. in PI, PII, Hassan et al. (2019), Lin et al. (2003) and Steele et al. (2017). In PI and PII, NDSI is derived from below-the-atmosphere observed reflectances, but it is evident that although the influence of the atmosphere would slightly increase the level of NDSI, the values where NDSI <0.1 would still be observed from snow-covered forest. In PI, the inverse atmospheric correction is carried out to the mast-borne data by SMAC (a simplified method for the atmospheric correction of satellite measurements in the solar spectrum) simulation (Rahman and Dedieu 1994), which increases the mast-borne NDSI, but negative NDSI values were still observed. In PI, the capability of MODIS-based NDSI to detect snow cover in dense forest on one specific day with full snow cover on the ground is demonstrated. The demonstration also shows that satellite-based NDSI <0.1 in dense forests along the Finnish-Russian border (Figure 15). Dense forests are also present in other parts of the boreal forest region, especially in Russia, and according to the results of PI and PII it is evident that the

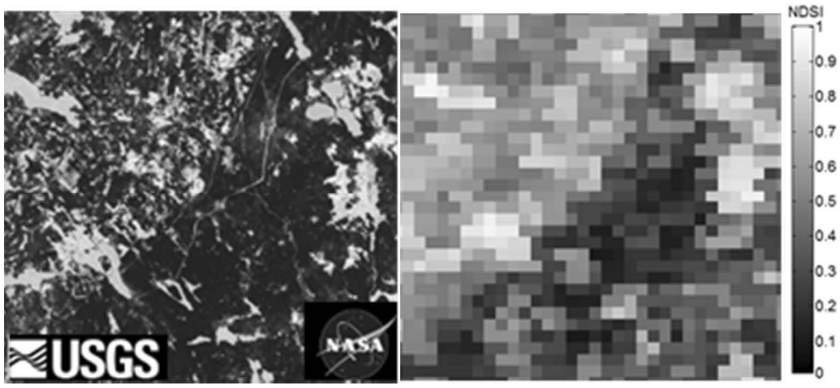

Figure 15. The performance of MODIS -based NDSI over fully snow-covered scene on 28 March 2003 (right) compared with Landsat/ETM+ scene acquired on 15 March 2003. These figures are adapted from PI, ©2012 Elsevier.

snow-covered area will be underestimated if the NDSI threshold is set to positive and other algorithms are not in use.

The results in PI and PII suggest that NDSI-based methods work more accurately in non-forested areas compared to forests. In PIV, the competence of NDSI in snow mapping when the ground is covered by thin melting snow layer often containing litter and snow-free patches is investigated. Figure 14 presents NDSI with respect to C from 5 May 2011 when a thin snow layer (*sd* <30 cm) covered the ground. Snow-free patches were discarded from the dataset. The NDSI provides significantly lower values compared to a thick snow layer (*sd* >70 cm) in all C classes. Remarkably, the mean NDSI is negative even in open areas (C <5%). Additionally, for thin snow, the NDSI variation is even higher and actually behaves the opposite way compared with the dry thick snow case; the variation increases when C decreases. In PIV, it was found that NDSI is dependent on land cover at the very end of the melting season when the snow layer is thin. For instance, the mean NDSI is -0.11 for transitional woodland/shrub on rocky soil (C=10–30%), while it is -0.55 for peat bogs. However, in addition to different mean NDSI for different land cover classes, internal variation for certain classes may be very high too. This fluctuation is caused partly by the heterogeneity of the snow layer (snow depth, grain size, amount of litter and emerging vegetation) and partly by the stronger effect of viewing and illumination geometry on the shortwave infrared reflectance compared to visible reflectance

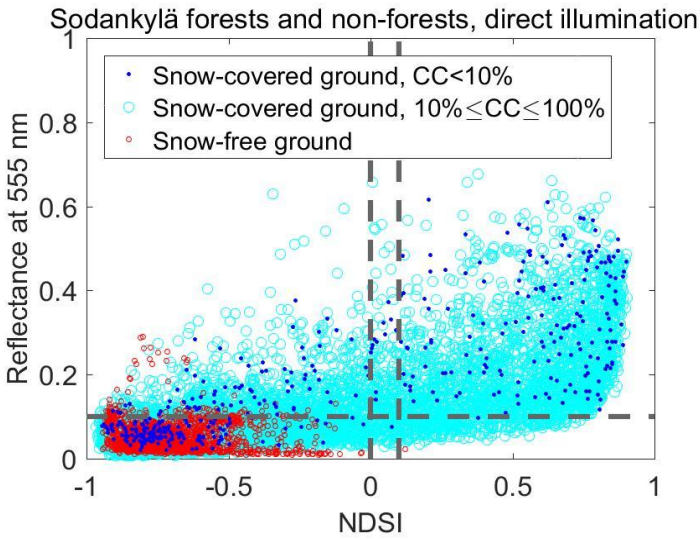

Figure 16. Airborne observations at 10 m resolution (5 May 2011) presented with the respect of threshold of MODIS C6 MOD10_L2 NDSI_Snow_Cover product. Dashed lines represent the thresholds of NDSI and Band 4 (555 nm) to identify snow in the pixel. Observations with snow-covered ground, snow depths <30 cm, are divided into two canopy cover (C) categories. This figure is adapted from PIV, ©2019 Elsevier.

(Table 3). Xie et al. (2006) investigated the effect of grain size on bidirectional reflectance and found a strong sensitivity at the NIR/SWIR wavelengths (>1.2 μm) while at visible wavelengths there was only very slight dependency between bidirectional reflectance and grain size. Peltoniemi et al. (2005b) investigated the bidirectional reflectance properties of the most common undergrowth species of boreal forest in Finland and found significant differences between the species but also within the same species. For instance, the set of spectra of lingonberry (*Vaccinium vitis-ideae*) measured at nadir and taken at various locations a few meters apart showed large variations in NIR and SWIR bands. Due to the emerging undergrowth through the thin snow layer, the variance in undergrowth bidirectional reflectance in SWIR wavelengths causes fluctuation in NDSI at the very end of the melting period. The unsteady behaviour of NDSI shown in the results of PIV indicates the weak performance of NDSI-based method for snow detection at the very end of the melting season both in forests and non-forests, particularly with

spectral bands for which the bidirectional reflectance effect may be notable. The NDSI data from 5 May 2011 in 10 m resolution is presented with respect to thresholds of NDSI and Band 4 (555 nm) in MODIS C6 MOD10_L2 NDSI_Snow_Cover product to identify snow in the pixel (Riggs et al. 2016) (Figure 16). In forests (C ≥10%) a threshold of NDSI >0 detected only 22% of the snow-covered pixels, while in the non-forests (C <10%) 45% of the snow-covered pixels were detected. Neither works as the threshold for green reflectance (Band 4 ≥0.11) which captures only 24% of snow-covered pixels where C ≥10% and 61% of snow-covered pixels where C <10%.

3.3 Scene reflectance in a boreal landscape: factors affecting the accuracy of snow extent mapping

3.3.1 Forest canopy

The influence of forest canopy on scene reflectance from snow-covered terrain is analysed in section 3.1. The noticeable effect of tree canopy on the modelled reflectance spectra is detected by comparing the resulting spectra of the linear mixing model and the observed spectra. A combination of the linear mixing model and the radiative transfer model showed notably better results than a single linear mixing model. Additionally the strong effect of canopy cover on reflectance is visible when airborne scene reflectances are analysed with respect to canopy cover (Figure 11). The influence of forest canopy on the observed reflectance is also visible when the observations contributed by snow-free canopy and snow-covered canopy are compared. In PI, the difference between the mast-borne reflectance from two dates, 18 March 2010 (snow-free canopy) and 21 March 2010 (snow-covered canopy), is found to be notable in visible wavelengths (Figure 17). The reflectance was almost twice as high at red bands for snow-covered canopy than for snow-free canopy. The tree canopy covers 48% of the observed area. The snow surface temperature and illumination conditions with cloud-free sky were similar on both days. In PII, the airborne reflectances from these two dates are compared. In PI and PII, the NDSI is found to be the most suitable measure to detect snow on the canopy. The relative NDSI difference between snow-free and snow-covered canopy varied from 32% (10%< C <30%) to 88% (70%< C <90%). However, when modelling FSC

this is not an issue because in snow on canopy conditions the ground is typically fully snow-covered; the slight increase of the observed reflectances inducing higher FSC may even compensate for the typical problem of underestimation of FSC in forests. On the other hand, in albedo mapping, the effect of snow on canopy should be taken into account.

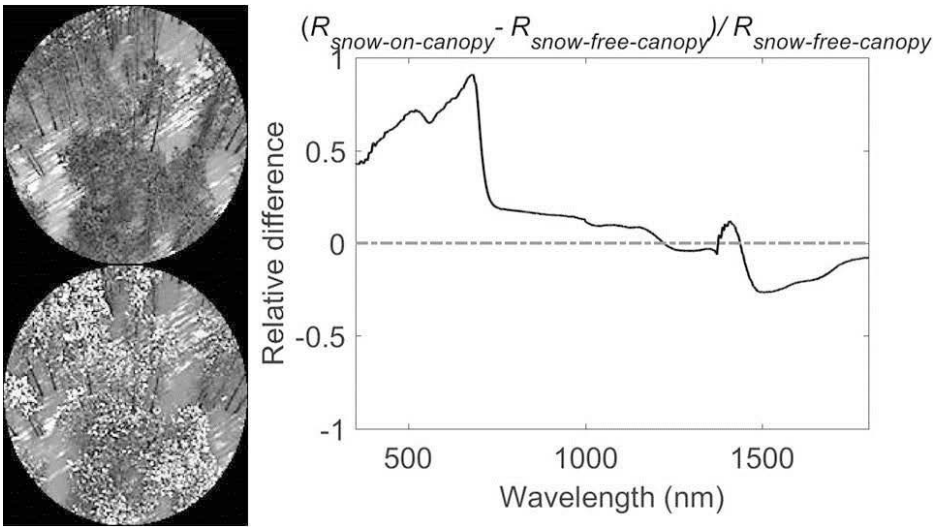

Figure 17. Left: The forest area observed by mast-borne spectroradiometer on 18 March 2010 with snow-free canopy and on 21 March 2010 with snow on canopy. Right: The relative difference between the spectra observed on these days. This figure is adapted from PI, ©2012 Elsevier.

3.3.2 Illumination geometry

The mast-borne spectroradiometer gives the possibility to investigate the effect of illumination geometry on the observed reflectance with the stable viewing geometry and canopy characteristics from a fully snow-covered forest. The spectra observed on 18 March 2010 are utilized in PI to investigate the variations in spectra during one day of non-changing snow conditions. The effect of solar azimuth on reflectance is found to be notable in all investigated wavelengths 350–1800 nm, thus the spectra were divided in scattering cases and backward scattering cases. Theoretically, snow scatters more in a forward direction (e.g. Painter and Dozier 2004; Peltoniemi et al. 2005a) whereas vegetation scatters more in a backward direction (Eklundh et al.

2007; Pellikka 1998; Peltoniemi et al. 2005b). However, Figure 18 illustrates how the spectral (backscatter) properties of tree canopy dominate the signal (Figure 18): the backward scattering produces higher reflectances at all wavelengths even though the canopy covers 40% of the observed land area (48% of the observed view). The difference between forward and backward scattering reflectances is highest in the NIR region. In PIII the effect of illumination geometry on mast-borne reflectance at the green band (555 nm) from the forest site is analyzed with the larger dataset; on 18 March 2010 and on twelve days between the 26 March 2013 and 12 April 2013. In PIII, as in PI, the higher reflectances in backscattering cases are found (Figure 19). Additionally, the results in PI and PIII indicate that the sun elevation has more of an effect in forward scattering cases (Figure 18 and 19). These findings encourage taking illumination conditions into account in FSC mapping from forests if nadir observations are not used.

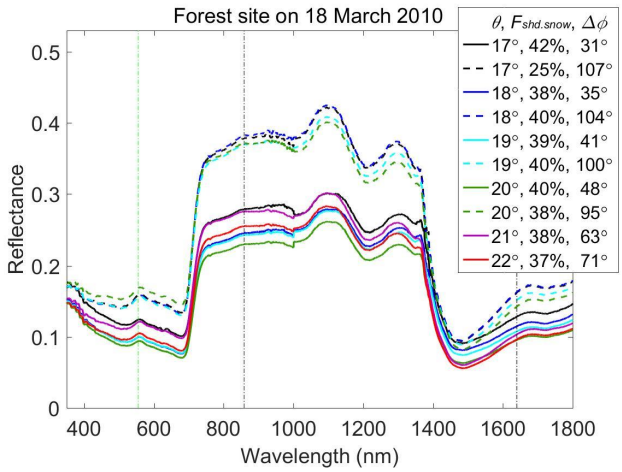

Figure 18. The mast-borne observations measured on 18 March 2010 when snow conditions were stable (several degrees minus) during the day. The forest covers 48% of the observed view. θ is sun elevation, $F_{shd.snow}$ is the fraction of shadowed snow and $\Delta\varphi$ is the relative azimuth. The sun is in the direction of the instrument view when $\Delta\varphi$ =0 (case of forward scatter). Dashed curves and solid curves represent backscattered and forward scattered spectra, respectively. This figure is adapted from PI, ©2012 Elsevier.

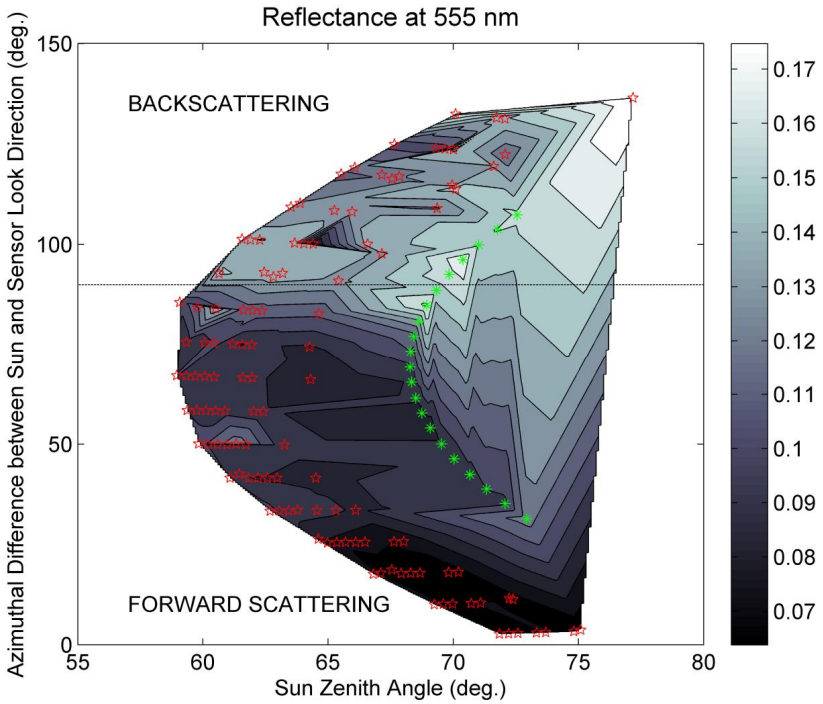

Figure 19. The mast-borne reflectances at the green band (555 nm) from the forest site presented with respect to the sun zenith angle and the azimuthal difference between the sun and sensor $\Delta\varphi$. The actual measurements during full snow cover conditions from 18 March 2010 are shown by green asterisks and measurements from 26 March – 12 April 2013 are shown by red pentagrams. The reflectance behaviour (contour plot) is interpolated from measurements at the locations of all the symbols. This figure is adapted from PIII, ©2014 Elsevier.

3.3.3 Melting snow cover

The behaviour of airborne reflectances at the very end of snow melting is investigated in PIV. In many previous investigations it was found that snow reflectance varies and decreases gradually during the melting process due to changes in the grain size, snow wetness, snow depth and the impurities in the snow layer (Dozier et al. 2009; Hori et al. 2017; Negi et al. 2010; Nolin and Dozier 1993; Pellikka and Rees 2010; Shekhar et al. 2018; Singh et al. 2010; Warren 1982; Warren and Wiscombe 1980; Wiscombe and Warren 1980). The low scene reflectances at the end of melting cause an underestimation in the FSC mapping. In PIV the effect of canopy cover and land cover class on the airborne reflectances observed at the very end of the snow melting is investigated. Consideration of the advantage of using this auxiliary information to improve the FSC estimates is presented. The measurements were made within one hour at nadir direction when the sky was cloud-free and the snow layer was heterogeneous with respect to grain size, snow wetness, snow depth and impurities. The results in PI–PIII point out the strong decrease of scene reflectance when the canopy cover (C) increases and blocks the view to the thick snow layer underneath the canopy. Figure 11 presents the observed airborne reflectance at the green band (555 nm) against the C in both cases: 1) snow layer is dry, *sd* >70 cm and 2) snow layer is melting, *sd* <30 cm. The results show that C does not affect the scene reflectance as strongly at the end of snow melting than dry thick snow cover conditions. At the very end of the melting season the heterogeneity of the wet thin snow layer causes higher variance on snow reflectance than canopy cover. The mean reflectances are low in all C classes producing a high correlation of variations (CV) (see PIV). Even in dense forests where the tree canopy obstructs the view to the snow layer, the mean reflectance is notably lower than in the case of a dry and thick snow layer. In PI the effect of snow metamorphosis on mast-borne reflectance in the forest site during the spring is also demonstrated. The hypothesis is that in diffuse illumination (i.e. at full cloud cover) the variation in reflectance is caused by actual changes in snow properties, because the forest stand and the illumination geometry can be assumed to be unchanged. The results of PI indicate that the effect of snow characteristics on reflectance is visible even when the canopy covers 48% of the observed view.

At the very end of the melting period the snow layer is partially transparent and the vegetation under the snow layer emerges through the thin snowpack. Thus the reflectance can be expected to behave differently in different land cover classes. In addition, the amount of impurities, such as needles which accumulates on the snow surface as a consequence of the upper snow layers melting, can be assumed to vary between land cover classes. In PIV, the reflectances measured with 80 cm spatial resolution on 5 May 2011 are compared with the 20 m resolution Corine Land Cover Classes (Härmä et al. 2015; Törmä et al. 2011). The land cover specific variation is visible when the ground is covered by a thin melting snow layer (Figure 20). However the internal variation within each class is high and hampers the utilization of land cover specific thresholds. Compared to the reflectances at NIR (859 nm) and SWIR (1640 nm) bands, at the green band (555 nm) the difference in correlation of variations (CV) between snow-covered and snow-free cases is notable (Figure 20). This information, i.e. high variation in reflectance at the green band, could be utilized to detect snow-covered areas at the very end of the melting season, since variation in reflectance is found to be very low at 555 nm in snow-free ground cases in all land cover classes. Additionally, the highest relative change between mean reflectance of snow-free and snow-covered cases are found at the green band (555 nm) in all land cover classes. The mean relative change of all classes at green band is 140% and is highest in the classes where C <10%. At the SWIR band (1640 nm), the transition from thin snow layer to snow-free ground induces both positive and negative changes in reflectance (Figure 20). This causes evident instability to an NDSI-based method for snow detection at the end of the snow melting season.

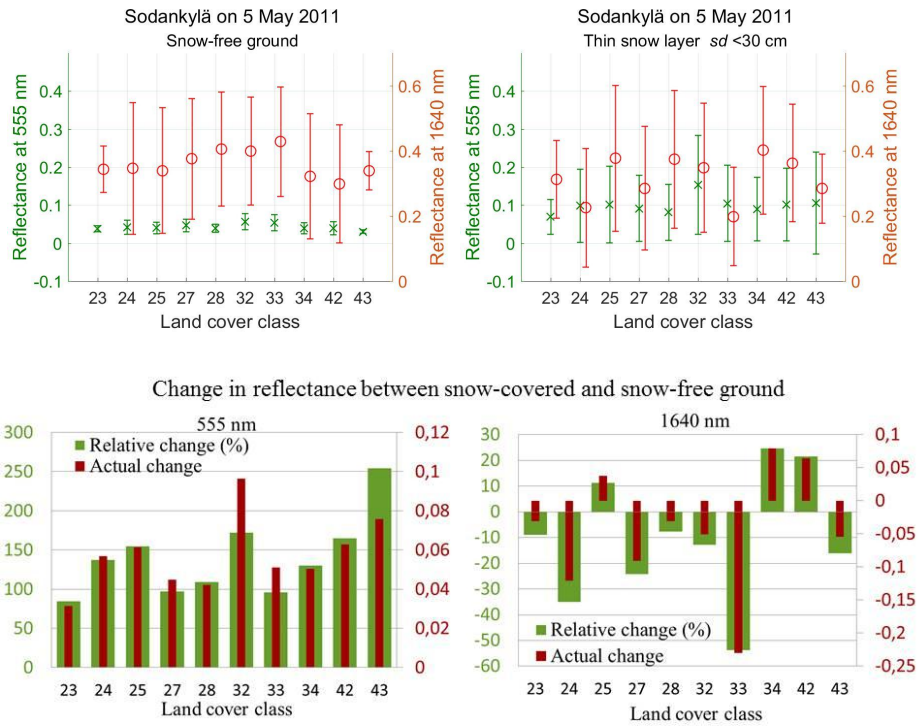

Code	Land cover class
23	Broad-leaved forest on peatland
24	Coniferous forest on mineral land
25	Coniferous forest on peatland
27	Mixed forest on mineral land
28	Mixed forest on peatland
32	Transitional woodland/shrub, cc <10%
33	Transitional woodland/shrub, cc 10–30%, on mineral soil
34	Transitional woodland/shrub, cc 10–30%, on peatland
42	Peatbogs
43	Peat-mining area

Figure 20. Upper pane: the mean and standard deviation of reflectances at 555 nm and 1640 nm. Left: snow-free areas. Right: areas covered by a melting snow layer (0 cm < *sd* < 30 cm). Lower pane: the actual change and relative change between these two cases for different CLC2012 classes at 555 nm and at 1640 nm. Analyses are based on the 80 cm resolution airborne reflectances from Sodankylä on 5 May 2011. These figures are adapted from PIV, ©2019 Elsevier.

4. Discussion and future aspects

The results in PI–PIV show the significant effect of the forest canopy on observed scene level reflectance from snow-covered landscape. In PI, the mast-borne reflectance from forest site in full snow-covered conditions is modelled and it is found that the modelled scene reflectance is more accurate when forest transmissivity is applied in the model (Figure 10). This is detectable when the modelling results by Salminen et al. (2009) from the same geographical land area are compared with the modelling results of PI. Salminen et al. (2009) applied a linear mixing model for wavelengths 350–1800 nm in fully snow-covered conditions. In their model they applied the reflectances of directly illuminated snow, shadowed snow and forest canopy and the areal proportions of these three parameters. The same linear mixing model is also used with the data set of PI. In both cases, the linear mixing model overestimated the reflectance considerably more, especially in visible wavelengths, than the advanced model where a zeroth order radiative transfer equation is combined with the linear mixing model. Additionally, the strong exponential correlation is found between the forest characteristics (C or V) and the observed visible reflectances above the canopy during dry snow conditions in PII and PIII (Figure 11 and 12). Actually, very similar reflectances are observed in dense forests with more than 70% of canopy cover, where the amount of the directly illuminated area can be assumed to be zero in high latitudes where light elevation angle is low, as in the Sodankylä study site. The results are in line with Ni and Woodcock (2000) who found that the snow-covered forest albedo varied dramatically as a function of canopy cover and they noticed that when canopy cover was more than 70% the presence of snow had only a minor effect on the observed albedo. These findings in PI, PII and PIII point out the necessity to apply a radiative transfer equation in snow mapping to describe the behaviour of reflectance in evergreen boreal forest with under-canopy snow.

The characteristics of satellite-borne data improve and advance with the advance of imaging technology. At the same time when new satellite instruments provides high/very high resolution data at a lower price and easy access or even at no cost, the available auxiliary data is more accurate and less expensive or even at no cost, as well. For example the LiDAR -based high resolution canopy cover data are already

freely available for many areas in Finland (www.nls.fi) whereas Copernicus HRL (High Resolution Layers) datasets include tree canopy density for Europe (https://land.copernicus.eu/). Global scale information on forests are provided e.g. by the European Space Agency (ESA) CCI Land Cover dataset (http://cci.esa.int). All these datasets are regularly updated. In PII and PIII, clear exponential correlation between canopy cover and reflectance is found. However, for the results in PIII, the pixel-level transmission more accurately defines the effect of the tree canopy on scene level reflectance from snow-covered terrain than information about canopy cover/volume since the heterogeneity of canopy within the pixel affects the interpretation of the model. The outcome also indicates that modelling results are a bit scale dependent when the canopy extinction coefficient is modelled using canopy cover/volume. E.g. the forest openings within the scene may not be properly considered because the canopy cover/volume is related to the forest patches only. In PI the effect of forest transmissivity on reflectance was observed in forest openings with shadows cast by pine trees.

In forests, the scene reflectance from snow-covered terrain also showed high variation according to illumination geometry (PI, PII, PIII). Compared to reflectances in the forward direction, the backward reflectances were notably higher and were less dependent on the sun zenith angle. This should be further investigated and take into account if nadir observations are not accessible. High variation in reflectances causes high variation in NDSI. In PI, it is found that in the forest opening the NDSI is similar in both illumination conditions, direct (i.e. clear sky) and diffuse (i.e. full cloud cover), while in the forest the NDSI difference is notable (Figure 13). This indicates that in open areas NDSI is able to reduce disturbances caused by variations in illumination geometry, but in forests the variation in illumination causes high variation in NDSI. The sensitivity of NDSI for illumination and viewing geometry in snow-covered forests is also found e.g. by Cao and Liu (2006) and Xin et al. (2012). In forests, even negative NDSI values are observed during full dry under-canopy snow conditions (PI, PII). Xin et al. (2012) have additionally found that NDSI can be negative even with snow on the ground because the presence of forest decreases the green reflectance significantly.

In PI and PIV, a considerable impact of melting snow on reflectances and NDSI is found, which needs to be taken into account in snow mapping during the melting season. It is also important to note that this applies to wide areas in the southern parts of the seasonal snow cover where snow layer, whenever is presented, is mostly thin and moist. Heterogeneity in snow cover at the end of the melting causes notable instability to the reflectances in the VIS, NIR and SWIR region causing inaccuracy of FSC retrieval. Importantly, this affects the capability of NDSI-based snow mapping methods too. The large variation in snow-covered reflectances hampers the utilization of different reflectance thresholds for different land covers. Actually, the variation in green reflectance could be utilized to capture snow-covered areas since variation is significantly higher for terrain covered by a thin melting snow layer than for snow-free terrain, independent of land cover type. Salminen et al. (2013) pointed out that land cover-specific ρ_{ground} values, especially for wetlands, could improve the performance of *SCAmod* when applied to extensive areas. Since in PIV heterogeneity in snow-covered ground reflectance is also found within single land cover classes, the suggestion in Salminen et al. (2013) is a more sufficient way to increase the accuracy of FSC retrievals than the utilization of land cover-specific thresholds at the end of the snow melting period.

The further exploitation of the extensive datasets presented in this thesis is particularly useful in developing spectral un-mixing methods and reflectance model-based snow and surface albedo monitoring techniques. That is, the applied airborne, mast-borne and ground-based hyperspectral optical reflectance data with different ground resolutions improve the understanding of the composition of the satellite scene reflectance behaviour and it's relation to the spectral signatures of natural ground targets. This would benefit the operative use of *SCAmod* for instance, as it would enable the local adjustment of model parameters, leading to increased accuracy of FSC-retrieval. In addition, the results of this thesis will benefit the accuracy assessment of the snow cover extent products and are already utilized in Salminen et al. (2018), in which a methodology to evaluate quantitative uncertainty characteristics of satellite data retrievals is developed. The dataset is acquired at relatively low solar elevation angles and needs further investigation before generalizing the results to work in areas where the sun elevation is clearly higher.

However, the dataset provides good quality reference information supporting the development of the optical snow mapping method and its further validation and regional parameterization.

5. Conclusion

Information on snow cover is important in hydrological, biological, and climatological aspects. However, the forest canopy hampers detection of snow-covered areas with optical satellite instruments. This thesis exploits multisensor reflectance data from different target resolutions providing unique and valuable information on the behaviour of scene reflectance from snow-covered forested terrain. The results allow the estimation of temporal (mast-borne data) and spatial variations (airborne data) of the scene reflectance in snow-covered boreal forests, and additionally provide the ground-based reflectances important for snow mapping. This thesis demonstrates that the utilization of a simple combination of a linear mixing model and a radiative transfer approach is a feasible method to predict reflectance properties in snow-covered forested terrain, given that detailed information on forest characteristics are available. The accuracy of the modelled satellite data retrieval can be additionally improved by applying more accurate, locally tuned target-specific reflectances as model parameters. The key findings of this thesis are:

- A non-uniform melting snow layer with varying impurities and snow depth causes significant variability and overall decrease in visible and near-infrared scene reflectances as well as NDSI in all land cover types. The effect of snow properties on scene reflectance is detectable even in the areas where canopy covers half of the observed view.
- In visible wavelengths variation in reflectance is distinctively high in snow-covered conditions at the very end of the snow melting period compared to snow-free conditions in all land cover types. Overall, reflectance at 555 nm is found to be most efficient in snow detection during the melting period due to its highest relative difference between snow-free and snow-covered reflectances compared to other wavelengths investigated and NDSI

- The effect of illumination geometry on reflectance and NDSI is found to be notable in snow-covered forested terrain. Tree canopy bidirectional reflectance properties dominate the signal even when snow covers half of the observed view. The effect of the sun zenith angle on scene reflectance from snow-covered forest is found to be higher in the forward scattering case than in the backward scattering case
- Snow on the canopy almost doubles the visible reflectances when the forest covers half of the view. Overall, the NDSI is found to be most suitable to detect canopy snow.
- Ground-based reflectances offers a feasible means to predict scene reflectance characteristics of snow-covered boreal forests observed by space-borne instruments. The forest canopy cover correlates exponentially with reflectances and in forests the non-linear radiative transfer approach describes the scene reflectance more accurately than the linear mixing model.
- Overall, the effect of the tree canopy on reflectance observations can be described realistically using simple forward models, which compensate the tree-canopy effect on the measured scene-level signal thus allowing the estimation on snow conditions beneath the canopy

These results support development of the optical snow mapping method, its further validation and regional parameterization. The results contribute significantly to improvement of the accuracy of optical data based snow cover products. However, further investigations are needed in the areas where the light incident angle is considerably higher.

References

ACIA. 2004. *Impacts of a Warming Arctic: Arctic Climate Impact Assessment. ACIA Overview report*. Cambridge University Press, Cambridge, UK.

AMAP. 2011. *Snow, Water, Ice and Permafrost in the Arctic (SWIPA): Climate Change and the Cryosphere*. Arctic Monitoring and Assessment Programme (AMAP), Oslo, Norway.

Cao, Y.-g. & Liu, C. 2006. Normalized difference snow index simulation for snow-cover mapping in forest by geosail model. *Chinese Geographical Science* 16(2), 171–175. doi: 10.1007/s11769-006-0013-6

Chang, A.T.C., Foster, J.L. & Hall, D.K. 1990. Satellite sensor estimates of northern-hemisphere snow volume. *International Journal of Remote Sensing* 11(1), 167–171. doi: 10.1080/01431169008955009

Chen, X., Liang, S., Cao, Y., He, T., & Wang, D. 2015. Observed contrast changes in snow cover phenology in northern middle and high latitudes from 2001–2014. *Scientific reports*, 5, 16820. doi: 10.1038/srep16820

Coakley, J. 2003. Reflectance and albedo, surface. In: Holton, J.R., Curry, J.A. & Pyle, J.A. (Eds.). *Encyclopedia of Atmospheric Sciences*. Academic Press, Amsterdam. pp. 1914–1923.

Cohen, J., Lemmetyinen, J., Pulliainen, J., Heinilä, K., Montomoli, F., Seppänen, J. & Hallikainen, M.T. 2015. The Effect of Boreal Forest Canopy in Satellite Snow Mapping-A Multisensor Analysis. *IEEE Transactions on Geoscience and Remote Sensing* 53(12), 6593–6607. doi: 10.1109/TGRS.2015.2444422

Derksen, C. & Brown, R. 2010. Spring snow cover extent reductions in the 2008-2012 period exceeding climate model projections. *Geophysical Research Letters* 39(19), L19504. doi: 10.1029/2012GL053387

Dietz, A.J., Kuenzer, C., Gessner, U. & Dech, S. 2012. Remote sensing of snow – a review of available methods. *International Journal of Remote Sensing* 33(13), 4094–4134. doi: 10.1080/01431161.2011.640964

Dozier, J., Green, R.O., Nolin, A.W. & Painter, T.H. 2009. Interpretation of snow properties from imaging spectrometry. *Remote Sensing of Environment* 113(Suppl. 1), S25–S37. doi: 10.1016/j.rse.2007.07.029

Eklundh, L., Jönsson, P. & Kuusk, A. 2007. Investigating modelled and observed Terra/MODIS 500-m reflectance data for viewing and illumination effects. *Advances in Space Research* 39(1), 119–124. doi: 10.1016/j.asr.2006.02.022

Frei, A., Tedesco, M., Lee, S., Foster, J., Hall, D.K., Kelly, R. & Robinson, D.A. 2012. A review of global satellite-derived snow products. *Advances in Space Research* 50(8), 1007–1029. doi: 10.1016/j.asr.2011.12.021

Gong, G., Cohen, J., Entekhabi, D. & Ge, Y. 2007. Hemispheric-scale climate response to Northern Eurasia land surface characteristics and snow anomalies. *Global and Planetary Change* 56(3-4), 359–370. doi: 10.1016/j.gloplacha.2006.07.025

Grenfell, T.C., Perovich, D.K. & Ogren, J.A. 1981. Spectral albedos of an alpine snowpack. *Cold Regions Science and Technology* 4(2), 121–127. doi: 10.1016/0165-232X(81)90016-1

Gutman, G.G. 1991. Vegetation indices from AVHRR: An update and future prospects. *Remote Sensing of Environment* 35(2-3), 121–136. doi: 10.1016/0034-4257(91)90005-Q

Haefner, H., Seidel, K. & Ehrler, H. 1997. Applications of snow cover mapping in high mountain regions. *Physics and Chemistry of The Earth* 22(3-4), 275–278. doi: 10.1016/S0079-1946(97)00143-2

Hall, D.K. & Riggs, G.A. 2007. Accuracy assessment of the MODIS snow products. *Hydrological Processes* 21(12), 1534–1547. doi: 10.1002/hyp.6715

Hassan, Q.K., Sekhon, N.S., Magai, R. & McEachern, P. 2012. Reconstruction of snow water equivalent and snow depth using remote sensing. *Journal of Environmental Informatics* 20(2), 67-74. doi: 10.3808/jei.201200221

Hendriks, J. & Pellikka, P. 2004. Estimation of reflectance from a glacier surface by comparing spectrometer measurements with satellite-derived reflectances. *Zeitschrift für Gletscherkunde und Glazialgeologie* 38(2), 139–154.

Hori, M., Sugiura, K., Kobayashi, K., Aoki, T., Tanikawa, T., Kuchiki, K., Niwano, M. & Enomoto, H. 2017. A 38-year (1978–2015) Northern Hemisphere daily snow cover

extent product derived using consistent objective criteria from satellite-borne optical sensors. *Remote Sensing of Environment* 191, 402–418. doi: 10.1016/j.rse.2017.01.023

Härmä, P., Hatunen, S., Törmä, M., Järvenpää, E., Kallio, M., Teiniranta, R., Kiiski, T. & Suikkanen, J. 2015. *GIO Land Monitoring 2011–2013 in the framework of regulation (EU) No 911/2010 - Final Report*. Finnish Environment Institute, Helsinki, Finland.

Jylhä, K., Tuomenvirta, H. & Ruosteenoja, K. 2004. Climate change projections for Finland during the 21st century. *Boreal Environment Research* 9, 127–152.

Kelly, R.E., Chang, A.T., Tsang, L. & Foster, J.L. 2003. A prototype AMSR-E global snow area and snow depth algorithm. *IEEE Transactions on Geoscience and Remote Sensing* 41(2), 230–242. doi: 10.1109/tgrs.2003.809118

Knipling, E.B. 1970. Physical and physiological basis for the reflectance of visible and near-infrared radiation from vegetation. *Remote Sensing of Environment* 1(3), 155–159. doi: 10.1016/S0034-4257(70)80021-9

Kuusisto, E. 1984. *Snow accumulation and snowmelt in Finland*. Publications of the Water Research Institute 55. National Board of Waters, Helsinki, Finland. http://hdl.handle.net/10138/31432

Lin, J., Feng, X., Xiao, P., Li, H., Wang, J., & Li, H. 2012. Comparison of Snow Indexes in Estimating Snow Cover Fraction in a Mountainous Area in Northwestern China. *IEEE Geoscience and Remote Sensing Letters*, 9, 725-729. doi: 10.1109/LGRS.2011.2179634

Malnes, E., Karlsen, S., Johansen, B., Bjerke, J., & Tømmervik, H. 2016. Snow season variability in a boreal-Arctic transition area monitored by MODIS data. *Environmental Research Letters,* 11, 125005. doi: 10.1088/1748-9326/11/12/12500

Marshall, S. & Oglesby, R.J. 1994. An improved snow hydrology for GCMs. Part 1: snow cover fraction, albedo, grain size, and age. *Climate Dynamics* 10(1), 21–37. doi: 10.1007/bf00210334

Mellander, P.-E., Loefvenius, M.O. & Laudon, H. 2007. Climate change impact on snow and soil temperature in boreal Scots pine stands. *Climatic Change* 85(1-2), 179–193. doi: 10.1007/s10584-007-9254-3

Mesarch, M.A., Walter-Shea, E.A., Asner, G.P., Middleton, E.M. & Chan, S.S. 1999. A Revised Measurement Methodology for Conifer Needles Spectral Optical Properties: Evaluating the Influence of Gaps between Elements. *Remote Sensing of Environment* 68(2), 177–192. doi: 10.1016/S0034-4257(98)00124-2

Metsämäki, S. 2013. *A fractional snow cover mapping method for optical remote sensing data, applicable to continental scale*. Monographs of the Boreal Environment Research 43. http://hdl.handle.net/10138/40183

Metsämäki, S., Mattila, O.P. & Niemi, K. 2012. Continental use of SCAmod fractional snow cover mapping method in boreal forest and tundra belt. In: *2012 IEEE International Geoscience and Remote Sensing Symposium (IGARSS'12)*. pp. 1578–1581.

Metsämäki, S., Pulliainen, J., Salminen, M., Luojus, K., Wiesmann, A., Solberg, R., Böttcher, K., Hiltunen, M. & Ripper, E. 2015. Introduction to GlobSnow SE-products with considerations for accuracy assessment. *Remote Sensing of Environment* 156, 96–108. doi: 10.1016/j.rse.2014.09.018

Metsämäki, S.J., Anttila, S.T., Huttunen, M.J. & Vepsäläinen, J.M. 2005. A feasible method for fractional snow cover mapping in boreal zone based on a reflectance model. *Remote Sensing of Environment* 95(1), 77–95. doi: 10.1016/j.rse.2004.11.013

Nagler, T., Rott, H., Ripper, E., Bippus, G. & Hetzenecker, M. 2016. Advancements for Snowmelt Monitoring by Means of Sentinel-1 SAR. *Remote Sensing* 8(4), 348. doi: 10.3390/rs8040348

Negi, H.S., Singh, S.K., Kulkarni, A.V. & Semwal, B.S. 2010. Field-based spectral reflectance measurements of seasonal snow cover in the Indian Himalaya. *International Journal of Remote Sensing* 31(9), 2393–2417. doi: 10.1080/01431160903002417

Ni, W. & Woodcock, C.E. 2000. Effect of canopy structure and the presence of snow on the albedo of boreal conifer forests. *Journal of Geophysical Research-Atmospheres* 105(D9), 11879–11888. doi: 10.1029/1999jd901158

Niittynen, P., Heikkinen, R.K. & Luoto, M. 2018. Snow cover is a neglected driver of Arctic biodiversity loss. *Nature Climate Change* 8(11), 997–1001. doi: 10.1038/s41558-018-0311-x

Nolin, A.W. & Dozier, J. 1993. Estimating snow grain size using AVIRIS data. *Remote Sensing of Environment* 44(2-3), 231–238. doi: 10.1016/0034-4257(93)90018-S

Nolin, A.W. & Dozier, J. 2000. A Hyperspectral Method for Remotely Sensing the Grain Size of Snow. *Remote Sensing of Environment* 74(2), 207–216. doi: 10.1016/S0034-4257(00)00111-5

Painter, T.H. & Dozier, J. 2004. Measurements of the hemispherical-directional reflectance of snow at fine spectral and angular resolution. *Journal of Geophysical Research: Atmospheres* 109, D18115. doi: 10.1029/2003JD004458

Painter, T.H., Rittger, K., McKenzie, C., Slaughter, P., Davis, R.E. & Dozier, J. 2009. Retrieval of subpixel snow covered area, grain size, and albedo from MODIS. *Remote Sensing of Environment* 113(4), 868–879. doi: 10.1016/j.rse.2009.01.001

Painter, T.H., Roberts, D.A., Green, R.O. & Dozier, J. 1998. The Effect of Grain Size on Spectral Mixture Analysis of Snow-Covered Area from AVIRIS Data. *Remote Sensing of Environment* 65(3), 320–332. doi: 10.1016/S0034-4257(98)00041-8

Panday, P.K., Williams, C.A., Frey, K.E. & Brown, M.E. 2014. Application and evaluation of a snowmelt runoff model in the Tamor River basin, Eastern Himalaya using a Markov Chain Monte Carlo (MCMC) data assimilation approach. *Hydrological Processes* 28(21), 5337–5353. doi: 10.1002/hyp.10005

Pellikka, P. 1998. Development of correction chain for multispectral airborne video camera data for natural resource assessment. *Fennia* 176(1), 1–110.

Pellikka, P., King, D.J. & Leblanc, S.G. 2000. Quantification and reduction of bidirectional effects in aerial cir imagery of deciduous forest using two reference land surface types. *Remote Sensing Reviews* 19(1-4), 259–291. doi: 10.1080/02757250009532422

Pellikka, P. & Rees, W.G. 2010. Glacier parameters monitored using remote sensing. In: Pellikka, P. & Rees, W.G. (Eds.). *Remote Sensing of Glaciers - techniques for topographic, spatial and thematic mapping of glaciers*. CRC Press, Leiden. pp. 41–66.

Peltoniemi, J.I., Kaasalainen, S., Näränen, J., Matikainen, L. & Piironen, J. 2005a. Measurement of directional and spectral signatures of light reflectance by snow.

IEEE Transactions on Geoscience and Remote Sensing 43(10), 2294–2304. doi: 10.1109/TGRS.2005.855131

Peltoniemi, J.I., Kaasalainen, S., Näränen, J., Rautiainen, M., Stenberg, P., Smolander, H., Smolander, S. & Voipio, P. 2005b. BRDF measurement of understory vegetation in pine forests: dwarf shrubs, lichen, and moss. *Remote Sensing of Environment* 94(3), 343–354. doi: 10.1016/j.rse.2004.10.009

Pulliainen, J. 2006. Mapping of snow water equivalent and snow depth in boreal and sub-arctic zones by assimilating space-borne microwave radiometer data and ground-based observations. *Remote Sensing of Environment* 101, 257–269. doi: 10.1016/j.rse.2006.01.002

Rahman, H. & Dedieu, G. 1994. SMAC: a simplified method for the atmospheric correction of satellite measurements in the solar spectrum. *International Journal of Remote Sensing* 15(1), 123–143. doi: 10.1080/01431169408954055

Rasmus, S. 2005. *Snow pack structure characteristics in Finland - measurements and modelling*. Report Series in Geophysics 48. University of Helsinki, Finland. http://hdl.handle.net/10138/23226

Riggs, G.A., Hall, D.K. & Román, M.O. 2016. *MODIS Snow Product User Guide to Collection 6 User Guide.* http://modis-snow-ice.gsfc.nasa.gov/uploads/C6_MODIS_Snow_User_Guide.pdf

Riggs, G.A., Hall, D.K. & Salomonson, V.V. 2006. *MODIS Snow Product User Guide to Collection 5*. http://modis-snow-ice.gsfc.nasa.gov/uploads/sug_c5.pdf

Rondeau-Genesse, G., Trudel, M. & Leconte, R. 2016. Monitoring snow wetness in an Alpine Basin using combined C-band SAR and MODIS data. *Remote Sensing of Environment* 183, 304–317. doi: 10.1016/j.rse.2016.06.003

Salminen, M., Pulliainen, J., Metsämäki, S., Böttcher, K. & Heinilä, K. 2013. MODIS-derived snow-free ground reflectance statistics of selected Eurasian non-forested land cover types for the application of estimating fractional snow cover. *Remote Sensing of Environment* 138(0), 51–64. doi: 10.1016/j.rse.2013.07.007

Salminen, M., Pulliainen, J., Metsämäki, S., Ikonen, J., Heinilä, K. & Luojus, K. 2018. Determination of uncertainty characteristics for the satellite data-based estimation of

fractional snow cover. *Remote Sensing of Environment* 212, 103–113. doi: 10.1016/j.rse.2018.04.038

Salminen, M., Pulliainen, J., Metsämäki, S., Kontu, A. & Suokanerva, H. 2009. The behaviour of snow and snow-free surface reflectance in boreal forests: Implications to the performance of snow covered area monitoring. *Remote Sensing of Environment* 113(5), 907–918. doi: 10.1016/j.rse.2008.12.008

Salomonson, V.V. & Appel, I. 2006. Development of the Aqua MODIS NDSI fractional snow cover algorithm and validation results. *IEEE Transactions on Geoscience and Remote Sensing* 44(7), 1747–1756. doi: 10.1109/tgrs.2006.876029

Schaepman-Strub, G., Schaepman, M.E., Painter, T.H., Dangel, S. & Martonchik, J.V. 2006. Reflectance quantities in optical remote sensing-definitions and case studies. *Remote Sensing of Environment* 103(1), 27–42. doi: 10.1016/j.rse.2006.03.002

Shekhar, C., Negi, H.S. & Srivastava, S. 2018. Correlation between effective snow grain size and hyper-spectral absorption peak characteristics – A case study over the North West Himalaya. *Remote Sensing Letters* 9, 1158–1166. doi: 10.1080/2150704X.2018.1516309

Shi, J.C., Dozier, J. & Rott, H. 1994. Snow mapping in alpine regions with synthetic aperture radar *IEEE Transactions on Geoscience and Remote Sensing* 32(1), 152–158. doi: 10.1109/36.285197

Singh, S.K., Kulkarni, A.V. & Chaudhary, B.S. 2010. Hyperspectral analysis of snow reflectance to understand the effects of contamination and grain size. *Annals of Glaciology* 51, 83–88. doi: 10.3189/172756410791386535

Solberg, R. & Andersen, T. 1994. An automatic system for operational snow-cover monitoring in the Norwegian mountain regions. In: *1994 IEEE International Geoscience and Remote Sensing Symposium (IGARSS'94)*. pp. 2084–2086.

Steele, C., Dialesandro, J., James, D., Elias, E., Rango, A. & Bleiweiss, M. 2017. Evaluating MODIS snow products for modelling snowmelt runoff: Case study of the Rio Grande headwaters. *International Journal of Applied Earth Observation and Geoinformation* 63(Suppl. C), 234–243. doi: 10.1016/j.jag.2017.08.007

Sukuvaara, T., Kyrö, E., Suokanerva, H., Heikkinen, P. & Suomalainen, J. 2007. Reflectance spectroradiometer measurement system in 30 meter mast for validating

satellite images. In: *2007 IEEE International Geoscience and Remote Sensing Symposium (IGARSS'07)*. pp. 2885–2889.

Thirel G, Salamon P, Burek P & Kalas M. 2013. Assimilation of MODIS Snow Cover Area Data in a Distributed Hydrological Model Using the Particle Filter. *Remote Sensing* 5(11), 5825-5850. doi: 10.3390/rs5115825

Turetsky, M., Abbott, B., Jones, M., Walter Anthony, K., Olefeldt, D., Schuur, E., Koven, C., David McGuire, A., Grosse, G., Kuhry, P., Hugelius, G., Lawrence, D., Gibson, C. & Britta K. & Sannel, A. 2019. Permafrost collapse is accelerating carbon release. *Nature* 569, 32–34. doi: 10.1038/d41586-019-01313-4

Törmä, M., Härmä, P., Hatunen, S., Teiniranta, R., Kallio, M. & Järvenpää, E. 2011. Change detection for Finnish CORINE land cover classification. In: *Earth Resources and Environmental Remote Sensing/GIS Aplications II*. SPIE Proceedings 8181. pp. 1–14.

Walter-Shea, E.A., Privette, J., Cornell, D., Mesarch, M.A. & Hays, C.J. 1997. Relations between directional spectral vegetation indices and leaf area and absorbed radiation in Alfalfa. *Remote Sensing of Environment* 61(1), 162–177. doi: 10.1016/S0034-4257(96)00250-7

Wang, G.X., Jiang, L.M., Wu, S.L., Shi, J.C., Hao, S.R. & Liu, X.J. 2017. Fractional Snow Cover Mapping from FY-2 VISSR Imagery of China. *Remote Sensing of Environment* 9(10), 983. doi: 10.3390/rs9100983

Warren, S.G. 1982. Optical properties of snow. *Rewievs of Geophysics and Space Physics* 20(1), 67–89. doi: 10.1029/RG020i001p00067

Warren, S.G. & Wiscombe, W.J. 1980. A Model for the Spectral Albedo of Snow. II: Snow Containing Atmospheric Aerosols. *Journal of the Atmospheric Sciences* 37(12), 2734–2745. doi: 10.1175/1520-0469(1980)037<2734:amftsa>2.0.co;2

Vikhamar, D. & Solberg, R. 2003. Subpixel mapping of snow cover in forests by optical remote sensing. *Remote Sensing of Environment* 84(1), 69–82. doi: 10.1016/S0034-4257(02)00098-6

Winther, J.-G. & Hall, D.K. 1999. Satellite-Derived Snow Coverage Related to Hydropower Production in Norway: Present and Future. *International Journal of Remote Sensing* 20(15-16), 2991–3008. doi: 10.1080/014311699211570

Wiscombe, W.J. & Warren, S.G. 1980. A model for the spectral albedo of snow. I: Pure snow. *Journal of the Atmospheric Sciences* 37, 2712–2733. doi: 10.1175/1520-0469(1980)037<2712:AMFTSA>2.0.CO;2

Woolley, J.T. (1971). Reflectance and transmittance of light by leaves. *Plant Physiology* 47, 656-662.

Xie, Y., Yang, P., Gao, B.-C., Kattawar, G.W. & Mishchenko, M.I. 2006. Effect of ice crystal shape and effective size on snow bidirectional reflectance. *Journal of Quantitative Spectroscopy and Radiative Transfer* 100, 457–469. doi: 10.1016/j.jqsrt.2005.11.056

Xin, Q.C., Woodcock, C.E., Liu, J.C., Tan, B., Melloh, R.A. & Davis, R.E. 2012. View angle effects on MODIS snow mapping in forests. *Remote Sensing of Environment* 118, 50–59. doi: 10.1016/j.rse.2011.10.029

Zarco-Tejada, P.J., Miller, J.R., Harron, J., Hu, B., Noland, T.L., Goel, N., Mohammed, G.H. & Sampson, P. 2004. Needle chlorophyll content estimation through model inversion using hyperspectral data from boreal conifer forest canopies. *Remote Sensing of Environment* 89(2), 189–199. doi: 10.1016/j.rse.2002.06.002

Journal Publications